POLITECNICO DI TORINO

Department of Mechanical and Aerospace Engineering

MSc Thesis
in Automotive Engineering

Modelling of the vibro-acoustic behaviour of transmission component using EFEM

Tutors
Prof. Eng. Alessandro Scattina

Candidate
Flavia Venuti

October 2020

A mamma e a papà.

Index

Preface

Thesis Introduction

This thesis has been performed during the Erasmus+ exchanged period in partnership with Rheinisch-Westfälische Technische Hochschule, University of Aachen.

The aim of this work is the modal analysis of three different transmission cross member by means of FE structure models and the validation of these models to be used in EFEM analysis.

In the first chapter, the main techniques and processes used in the acoustic field to investigate the behaviour of models in the frequency domain will be pointed out, with a particular focus about the FEM analysis on discretised structures and then the processes to perform an EFEM analysis.

In the second chapter, the development of all the models will be done, the major challenges will be underlined and the first analyses will be performed: a modal analysis to get the resonance frequencies and different mode shapes of the structures. After all, the relationships with the results obtained from the simulation with other coming from real measurements will be compared. In order to fulfil perform the analyses, the NVH software present in Hypermesh will be used and the MAC matrices will be found out.

Then, the EFEM development simulation will be explained, including the main issues that can be found and the steps followed to perform it.

In the last chapter, the results will be shown, analysed, compared and possible improvements will be discussed.

1 Chapter 1

1.1 Fundamentals

Noise is mainly classified into airborne and structure-borne noise. The first one consists of the progressive movement of mass particles, i.e. vibrations, and is transmitted in the form of sound waves at the speed of sound (roughly 344m/s in air). The differing frequencies (n of changes in pressure per second) generate characteristic tones. Frequencies are measured in Hertz (Hz). The audible range of a healthy young person extends approximately from 20Hz to 20 kHz. Structure-borne noise is transmitted through solid structures, such as steel, wood, concrete, stone etc. This includes for example impact sound and part of the noise generated by the technical machinery installed in a building.

This chapter clarifies main aspect of sound characteristics and properties, guiding the reader into main aspect of the numerical methods employed in acoustics. The finite element method and their processes are explained, as well as the modal analysis and how this one is performed by means of software. At the end, purposes and processes about energy based finite element method will be illustrated.

1.2 Sound characteristics

Sound, or noise, is the result of pressure variations, or oscillations, in an elastic medium, generated by a vibrating surface or turbulent fluid flow. In gases and fluids, sound propagates in the form of longitudinal waves, involving a succession of compression and rarefaction. However, in solid state bodies it propagates as transverse waves in addition to longitudinal waves.

The figure below shows the pressure oscillations of a sound wave. The amplitude of pressure changes, which is described by the root mean square (RMS) amplitude, expressed in Pascal (Pa):

$$p_{eff} = \sqrt{\frac{1}{T}\int_0^T p^2(t)dt} \qquad \textit{Eq. 1}$$

The wavelength λ is the distance travelled by the pressure wave during one cycle, the frequency f is the number of cycles per second expressed in Hertz (Hz), the period T is the time taken for one cycle of a wave to pass a fixed point that is the inverse of the frequency.

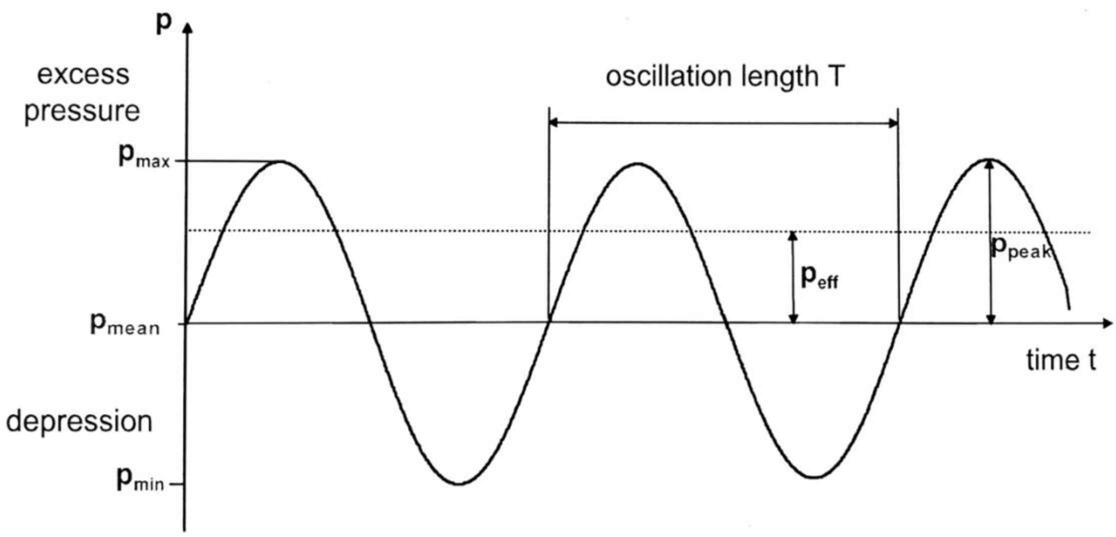

Figure 1. Pressure oscillations of a sound wave [BIE12]

There are various types of sound fields, namely free field, near field, far field, direct field and reverberant field. The free field is a region in space where sound may propagate free from any form of obstruction. The near field of a source is the region close to a source where the sound pressure and acoustic particle velocity are not in phase. The near field is limited to a distance from the source equal to about a wavelength of sound or equal to three times the largest dimension of the sound source, whichever is the larger. The far field of a source begins where the near field ends and extends to infinity. The direct field of a sound source is defined as that part of the sound field that has not suffered any reflection from any room surfaces or obstacles. The reverberant field of a source is defined as that part of the sound field radiated by a source that has experienced at least one reflection from a boundary of the room or enclosure containing the source. The sound pressure level (SPL) is represented:

$$L_p = 10log\frac{p^2}{p_0^2} = 20log\frac{p}{p_0}\ [dB] \qquad \textit{Eq. 2}$$

where $p_0 = 2 \cdot 10^{-5}$Pa, which is the minimum sound pressure perceived by human beings (threshold of audibility). The maximum value is about 200 Pa (threshold of pain). The following figure shows an overview of SPL values for various sounds.

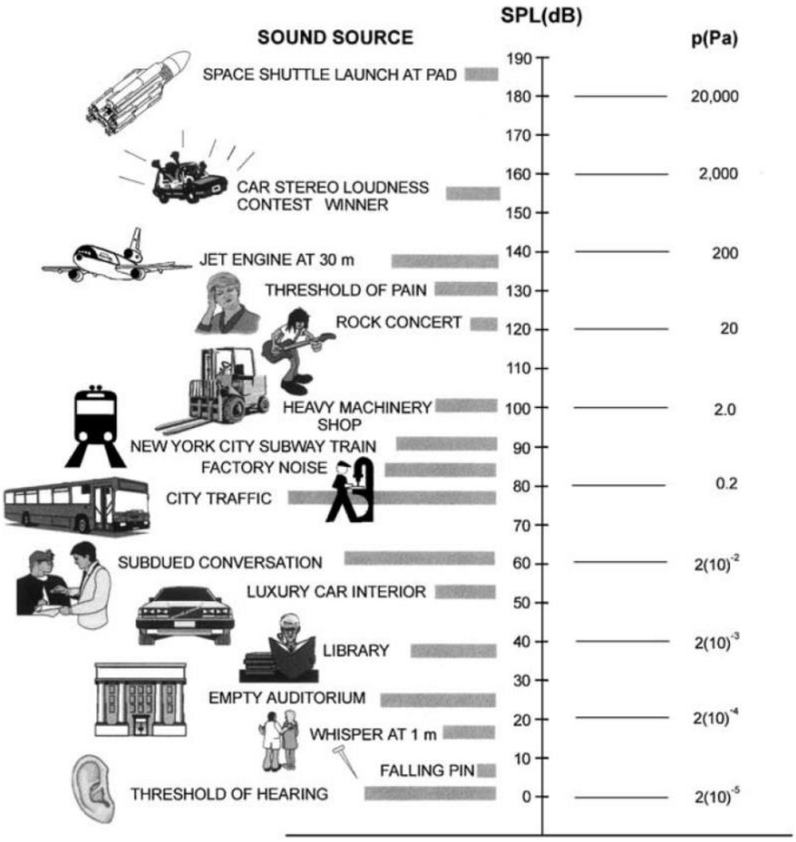

Figure 2. Sound pressure levels and corresponding pressures of various sound sources [RAI06]

Figure 1 illustrates the range of the decibel scale compared with already known sound sources, in particular the range from 0 up to 50dB is comforting for the human, while the one from 50 up to 90 irritates. Above that level human can overcome the threshold of pain and severe injuries can occur.

The frequency also has a great influence on the oscillation perception of humans. There is a frequency-dependent relation between physical measurements and subjective perception, which differs based on the separate body parts and effective directions. Analyses have shown that the perception of humans crosses over from a sensible to an audible area. The exact relation is shown in the following figure. Structure-borne noise is perceived from about 0.8-1 to about 70-100Hz. The audible perception increases its relevance above this frequency area. The transition zone is called harshness.

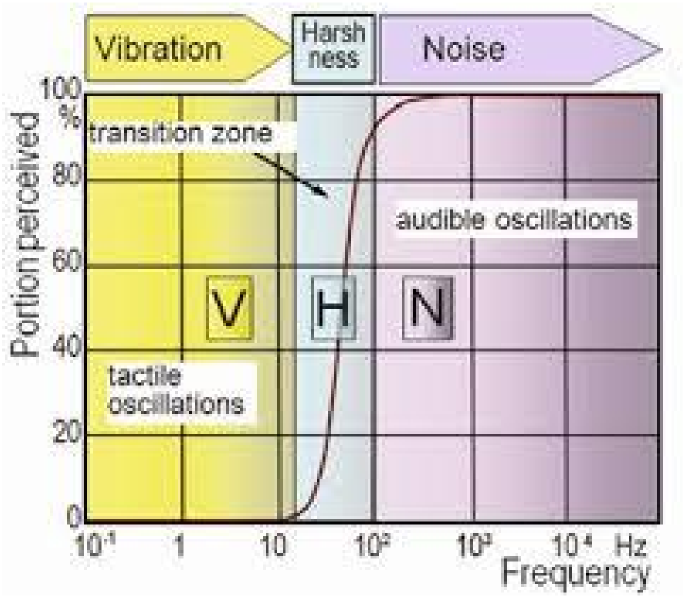

Figure 3. Noise, Vibration and Harshness, sound vs frequency [HEI11]

For the analysis of sound transfer and propagation, several measurement and calculation procedures have been developed. The method that is commonly used is experimental modal analysis that will be explained in the following chapter.

1.3 Experimental Modal Analysis

Experimental modal analysis is carried out to determine the characteristic mode forms and the corresponding Eigen frequencies of the measured component from the eigenvectors. The

Eigen frequencies are the frequencies at which the structure normally tends to vibrate if it has already been deformed and is let free to vibrate on its own.

When a structure is excited in wide frequency range, the actual physical displacement, in each point, is exactly the combination of all the mode shapes of the structure. With harmonic excitation close to a modal frequency, 95% of the displacement may be due to that particular mode shape. Nevertheless, a mode shape is an inherent dynamic property of a structure in free vibration, thus when no external load is applied. It represents the relative displacements of all parts of the structure for that particular mode. This concept can be better understood if considering the example of a plate fixed at an end.

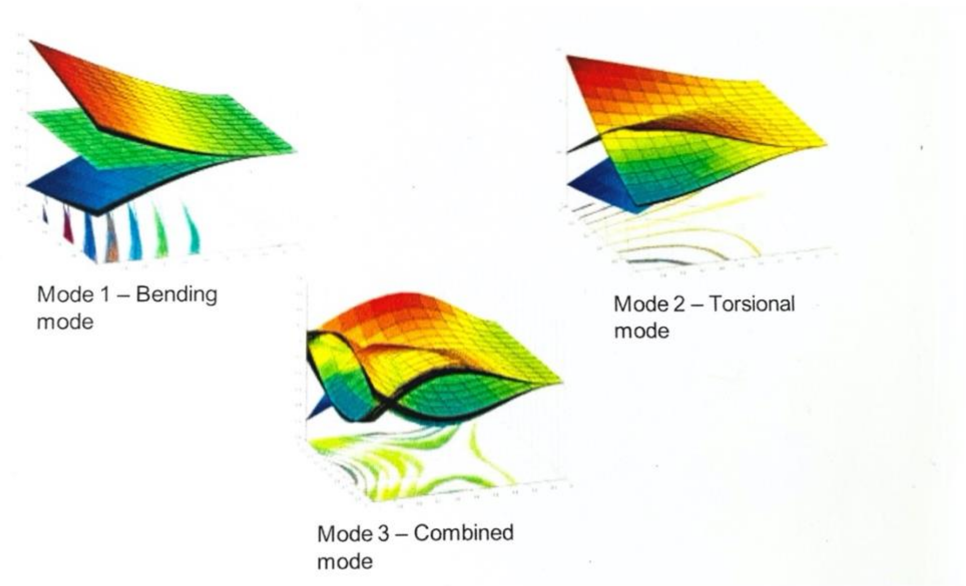

Figure 4. Mode shapes of a plate fixed at an end [ADH15]

In order to experimentally determine the modal parameters and therefore mode shapes of a structure, has to be suspended with elastic ropes or air springs. At an initiation point, impulsive force excitations with an impulsive hammer or harmonic force excitations by a shaker are applied. Accelerometers are attached at a certain points of the structure to record the resulting response as time signals. These signals can be converted into frequency responses by means of the Fourier transformation. The latter is an algorithm that samples a signal over a period of time and divides it into its frequency components.

The transfer functions (H(s)) are then computed as:

$$H(s) = \frac{Y(s)}{X(s)} \qquad \text{Eq. 3}$$

Modal parameters are identified by curve fitting the obtained set of transfer functions. This is done by minimizing the squared error between the analytical function and the measured data. Single degree of freedom (SDOF) and multiple degree of freedom (MDOF) methods are the local methods commonly used for this purpose. Global and Multi-Reference methods are the global methods used. SDOF methods estimate modal parameters for one excitation at a time while MDOF, Global and Multi-Reference can simultaneously estimate modal parameters for two or more excitations at a time.

1.4 Normal modes analysis

Normal modes analysis is the process of determining the modal parameters namely modal frequency, modal damping and mode shape of a structure for all the modes in the frequency range of interest. Modes are properties of a structure that are determined by the material properties and the boundary conditions of the structure. If they will be varied, even the modes of the structure will change as well.

Modes can be classified into normal modes and complex modes. A normal mode of an oscillating system is the motion in which all parts of the system move in a sinusoidal way with the same frequency and with a fixed phase relation. Therefore, the modal displacements result in real and positive or negative. Instead, complex modes can have any phase relationship between different parts of the structure. They are complex and can have any phase value.

To easily understand the concept of normal modes analysis the idea of single degree of freedom (SDOF) can be employed. The SDOF, commonly known as spring-mass-damper system, is described by the following equation:

$$M\ddot{x}(t) + C\dot{x}(t) + Kx(t) = f(t) \qquad \text{Eq. 4}$$

M is the mass matrix, *C* is the damping coefficient and *K* is the stiffness matrix. The sum of the forces acting on the mass *M* should be equal to zero. The first term of the equation represents the inertial force, while second and third terms represent the damping force and the restoring force. The term on the left, instead, represents the externally applied force. The variable *x(t)* represents the position of the mass with respect to its equilibrium point.

In order to study it, the Laplace transformation represented in the following equation is used:

$$Z(s)X(s) = F(s) \tag{Eq. 5}$$

The Z(s) represents the dynamic stiffness as shown in Eq. 6.

$$Z(s) = ms^2 + cs + k \tag{Eq. 6}$$

The transfer function *H(s)*, inverse of the dynamic stiffness (Eq. 6), evaluated between displacement and force related, is calculated in the equation Eq. 8

$$X(s) = H(s)F(s) \tag{Eq. 7}$$

$$H(s) = \frac{1}{ms^2 + cs + k} \tag{Eq. 8}$$

The poles of the system, evaluated in order to study the stability of the system, are the roots of the equation Eq. 7. In mechanical structures, the damping coefficient *c* is usually very small resulting in a complex and conjugate pole pair represented by the equation Eq. 9.

$$\lambda = -\sigma \pm i\omega_d \tag{Eq. 9}$$

At this point, the damped natural frequency can be indicated, as well as the undamped natural frequency:

$$f_d = \frac{\omega_d}{2\pi} \tag{Eq. 10}$$

$$f_n = \frac{\omega_n}{2\pi} \tag{Eq. 11}$$

Where:

$$\omega_n = \sqrt{\frac{k}{m}} = |\lambda| \qquad \textit{Eq. 12}$$

Moreover, the damping ratio is expressed in the following as:

$$\zeta = \frac{c}{2m\omega_n} = \frac{\sigma}{|\lambda|} \qquad \textit{Eq. 13}$$

By substituting the previous formulas, the damped natural frequency can be expressed even in a different way:

$$f_d = f_n\sqrt{1-\zeta^2} \qquad \textit{Eq. 14}$$

The common algorithms used in FE NVH simulations to compute the eigenvalues are Lanczos and AMSES method. Since in this work only the first one will be used, an explanation just on that one will be given.

The Lanczos algorithm is a direct algorithm devised by Cornelius Lanczos that is an adaptation of power methods to find the most useful eigenvalues and eigenvectors of an n^{th} order linear system. To find eigenvalues of a matrix *H* of dimension *N*, Lanczos method requires the evaluation of matrix-vector products $H \cdot v$ as the only problem-specific step. This matrix-vector product can be calculated particularly efficiently when the matrix *H* is sparse, thus when the number of non-zero matrix elements per row does not scale with the matrix dimension. Storing such a matrix takes only *O(N)* memory and $H \cdot v$ can be evaluated in *O(N)* time. Calculating the extremal eigenvalues requires *O(1)* iteration, i.e. overall *O(N)* time. For comparison, a direct diagonalization takes *O(N2)* for storing the matrix and *O(N3)* time to diagonalise. Besides their favourable scaling for sparse matrix problems, iterative methods have the advantage that they systematically approach the desired result. Typically, the iteration converges geometrically and can be stopped as soon as the desired accuracy is reached. In contrast, direct methods appear to make no progress towards the solution until all *O(N3)* operations are completed and the full result is obtained. Spectral functions are calculated in the recursion method. The great advantage of this approach is that it gives the dynamical properties of the ground state directly on the real axis. The price is the restriction to finite-size systems. The EIGRL bulk data entry can be used to activate the Lanczos eigen solution. The EIGRL card defines data required to perform real eigenvalue analysis (vibration or buckling) with the Lanczos method.

1.5 Numerical methods in acoustics

The analysis methods described so far are applied on real structures, often prototypes. Since fulfilling acoustic requirements through major design changes in the prototype stage is difficult, modern calculation methods are implemented in the beginning of the design stage. The Finite Element Analysis (FEA) as well as the Energy-based Finite Element Analysis (EFEM) are two methods utilized in acoustic analysis and they will be employed in the work described in this thesis.

FEA is the most commonly used method in acoustic analysis. A FE model is made up of solid and shell elements with known properties. Those elements are then addressed to the whole model employed for the simulation. A set of differential equation describes the behaviour of each element present in the model, and even considering the boundary conditions applied and the constraints as well; through those equations, the software is able to compute the displacements at the nodes of the elements.

The FEA calculation method is a deterministic one. The physical state variables are shown at each node. The calculation of these variables inside the vehicle is done using a modal approach. For acoustic analysis of vehicle interiors, it is sufficient to detect the spatial and temporal average acoustic behaviour in the frequency bands for each individual subsystem.

The Energy Based Finite Element Method, also known as EFEM is used to evaluate the vibrational behaviour in the high frequency domain. Numerical discretization methods like FEM and BEM (Boundary Element Method) are the most conventional tool widely used to predict first modes of the structure and frequency response functions. Those two methods are employed mainly in the investigations at low and medium frequencies but instead, at high frequencies, because of the shorter wavelengths and higher modal density, they are not suit enough. In FEM the number of elements should be increased and this makes the computation more costly. So far, new tools have to be employed to avoid problems of result resolution and even computation time and SEA, Statistical Energy Analysis, finds a big role in it.

SEA divides a complex system into a certain number of subsystems. Working with the energy that is exchanged between subsystems and the dissipated within them, the acoustic response can be evaluated.

EFEM, works with the energy balance, discretizing the model with finite elements. The energy flow within the components can thus easily computed by means of the single elements.

1.5.1 FEA approach and process

FEA plays a vital role in design decisions during the early development of a vehicle. At first, the approach of FEA is described and then the process of FE calculation follows it. After this, the numerical modal analysis takes place, which describes the structural behaviour of a component and as a last step, the frequency response analysis is studied.

All the mechanical systems can be transformed into an adequate analogous model. During the modelling process, the mathematical description of a system should be as simple as possible but also as realistic as necessary. In the case of simple mechanical models, an analogous model can be developed by using the classic approaches of mechanics.

The modelling in the case of a mechanical system can be represented as follows:

1) Mechanical system
2) Substituted mechanical system
3) Mathematical description
4) Problem solving

The modelling can be categorized into the discrete and the continuous concept. Discrete modelling is dependent on a finite number of linear equations, while the solution of a continuous model results from the solution of differential equations, which is only possible in cases of simple models. But actually, most of the times, really complex models are present, characterized by complex geometry, super positioned loads, nonlinear behaviour of the material and so on. To solve those types of systems, a continuous approach is inadequate and it becomes necessary to use the finite element method, also known as FEM, to find a solution. The idea of not describing the considered system as a whole, but instead by dividing it into small, finite elements linked together at the edges of the elements, is the basic idea of the FEM. The process that lead from the continuum, which is a composition of small incremental areas, the finite elements, to the discrete way is exactly the discretization process.

The main purpose of the FEM consists of converting the problem describing differential equation into a linear set of equations. The basic equation of each FEM is the elementary stiffness equation

$$F = k \cdot u \qquad \textit{Eq. 15}$$

Using a vector F of the outer loads that acts on an element node and the material properties summarized in the factor k, the deformation vector u is evaluated. With the set of equations, the characteristic values of displacements, rotations, strains, stresses, forces and torques can be determined. Considering mass and damping of a mechanical system, results in a second order differential equation is represented.

$$M \cdot \ddot{u}(t) + C \cdot \dot{u}(t) + K \cdot u(t) = F(t) \qquad \textit{Eq. 16}$$

M is the mass matrix, C is the damping matrix and K is the stiffness matrix. Based on this equation, dynamic procedures can be analysed.

The entire process of FE calculation can be divided into four main stages: the CAD system, the pre-processor, the solver and in the end the post processor. The first stage involves the creation of a geometrical structure model. Then there is the generation of the FE model by use of a pre-processor. The structure is then meshed, material properties are defined and the respective boundary conditions and loads are applied. There are various pre-processing solvers that set up the stiffness matrix and calculate the solution of the problem describing the system of equations. A post processor is a helpful tool that by means of an algorithm is able to visualise the data coming from the results: images, graphs and so on. It allows to study the results coming from the simulations, focusing, if needed, only on one part of the model or the whole one. It is able to colour the model depending on the gradient of the entities analysed, in order to help to have a better visualization of them. For the current work, in the final stage, the results by means of displacements and stresses are visualised and analysed. The one that is used in this work is HyperView.

The element types can be subdivided into dimensionless point elements, one-dimensional (1D) line elements, two-dimensional (2D) shell elements and three-dimensional (3D) volume elements. Rod and beam elements are one-dimensional line elements. They are employed in those cases in which one dimension is significantly larger than the two other dimensions. The simplification by rod and beam elements provides meaningful results for systems that have cross section smaller than one tenth of the structure length. The difference between a beam element and a rod element lies in the number of degrees of freedom. While the rod element can only translate, the beam is able to rotate of a certain angle around its own longitudinal axis.

2D shell elements provide better results than volume elements in those cases in which one dimension (for example the thickness) is significantly smaller than the other two dimensions, so that the stresses in the direction of the thickness are negligible. 3D volume elements, instead, are used in complex solid components and can fill out a component as either a tetrahedral (4nodes), pentahedral (6nodes) or hexahedral (8nodes). The main differences and shapes are reported here below, following a differentiation between 2D shell and 3D volume elements.

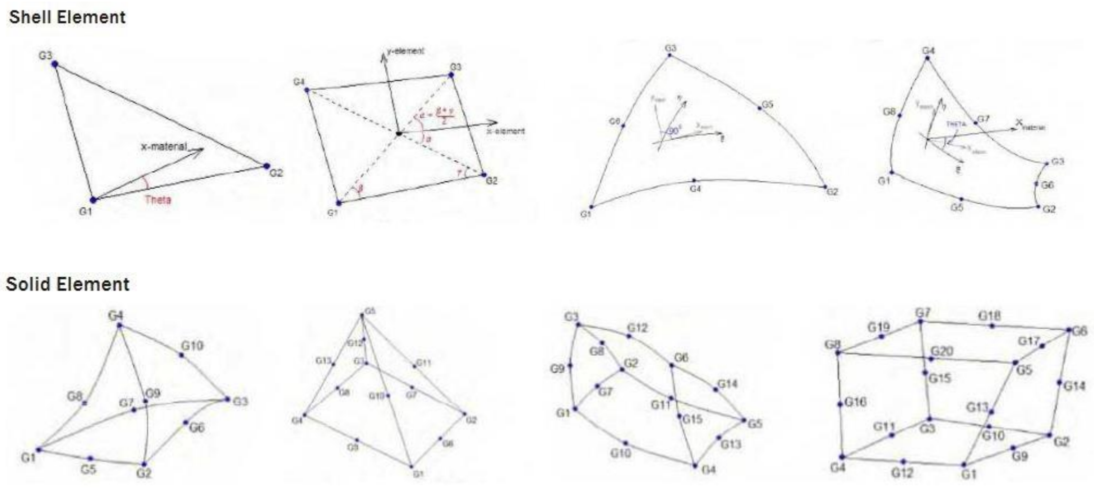

Figure 5. Example of mesh elements [ALT18]

The 2D elements have a distinction between triangular and quadrilateral elements. Similarly, an analogous differentiation is made in the 3D elements between tetrahedral and rectangular elements. The last difference is based on the choice of the structure order. In the linear approach, nodes only exist at the corner of the element while in the quadratic approach there is an additional node between the vertices. The behaviour of the elements respectively of their element nodes is described by a shape function. Those functions show displacements and tensions for the actual area.

In order to enable the connections between the various component meshes, there are connector elements such as WELD, RBE2 or RBE3 (Rigid Body Element) and RDE. The WELD element represents a weld or fastener connecting two surface patches or points. The RBE2 element is a rigid, dimensionless and massless element and consists of one so-called independent node and any number of so-called dependent nodes. The independent node is a reference point whose displacements have a rigid and direct effect on all connected nodes (dependent nodes). The transmitted forces and patterns are distributed to all dependent nodes. Modelling by means of the RBE2 element is a numerically very robust method for directly and rigidly connecting nodes to each other.

All the above-mentioned elements are used to generate a mesh. Mesh generation is the practice of generating a mesh that approximates a geometric domain. To save calculation time and create a mesh component as much as possible closer to the original geometry, it is important to simplify the model as much as possible, by deleting the unnecessary lines that would interfere with the creation of the meshes or would compromise the quality. Meanwhile the model has stay as detailed as necessary. When meshing, first the surfaces are chosen, then the element size is defined and afterwards the mesh is generated. While meshing a structure, it is important to check the element quality: areas of the structure with large load applications should be meshed as fine as possible in order to increase the accuracy of the calculation. Areas where only a small load application is expected can be meshed more roughly. By means of the interactive command, instead, is possible, after selecting a surface, to choose the size and the position of the meshes as well. The final step of meshing is the definition of contacts if the investigated load case requires nonlinear FEA to be performed.

1.5.2 EFEM approach and process

The equations that rule EFEM method are based on the principle of energy conservation, thus considering the energy exchanged and dissipated within the elements. In order to evaluate it, a control volume V in steady state conditions is considered and the energy conservation is expressed as in:

$$\pi_{in} = \pi_{diss} + \nabla\bar{q} \qquad \textit{Eq. 17}$$

Where π_{in} is input power density, π_{diss} is the dissipated power density and $\bar{q}$ is the intensity or energy flow at the borders of the subsystem. The dissipation of the energy can be caused by different kind of phenomena, and as a general rule it can be expressed by the damping loss factor of the material, as:

$$\pi_{diss} = \eta\omega e \qquad \textit{Eq. 18}$$

ω represents the angular frequency and e is the time and space averaged energy density. Neglecting the near field inside the control volume and instead considering only the flexural waves in plates, the averaged power flow $\bar{q}$ can be derived and it is proportional to gradient of the time and space averaged energy density.

$$\bar{q} = -\frac{c_g^2}{\eta\omega} \cdot \nabla e \qquad \textit{Eq. 19}$$

The group speed of bending waves in plates c_g is calculated separately for each wave type and depends both on material and on geometric properties of a structure or fluid. By combining the previous equations, it can be obtained:

$$\pi_{in} = -\frac{c_g^2}{\eta\omega} \cdot \nabla^2 e + \eta\omega e \qquad \textit{Eq. 20}$$

The energy conservation equation (Eq. 17) can be solved using finite element discretization. Discontinuities that exist between the elements, such as those one present in the material, will lead to a discontinuity in the energy densities and thus they have to be avoided. In order to do so, joint elements are created in the structure (see **Figure 6.** Coupling of two elements at a discontinuity [HÜS18]) and will be added in the term Q to the EFEM´s equation system:

$$\{F\} + \{Q\} = [K] \cdot \{e\} \qquad \textit{Eq. 21}$$

The matrix $[K]$ is a function of each element´s group velocity, damping loss factor and the angular frequency. The vector $\{F\}$ contains the external time averaged input power densities π_{in} for each node. The coupling vector $\{Q\}$ describes the power flow across the perimeter of elements coupled at a discontinuity. Considering two infinitesimal elements i and j,

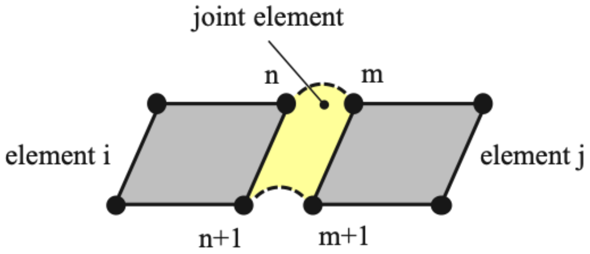

Figure 6. Coupling of two elements at a discontinuity [HÜS18]

Infinitesimally speaking, Eq. 21 can be applied at different nodes (n and m) for the different elements (i and j)

In order to predict the radiation noise of the structure and the resulting sound pressure level at a certain distance, the structure has to be coupled with an acoustic cavity (**Figure 7.** Coupling of a plate element and an acoustic cavity [HÜS18]).

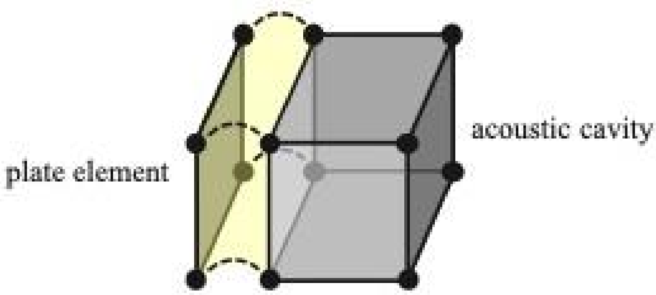

Figure 7. Coupling of a plate element and an acoustic cavity [HÜS18]

To couple a plate element with an acoustic cavity, extra nodes have to be added so to predict different energy densities values for bending waves both in the plate element and the acoustic as well. Then a coupling matrix has to be added to the global system matrix from the transmission coefficients. To calculate those coefficients, a diffuse wave field is assumed and the transmission coefficients will be then functions of the geometry, material properties and the structure´s radiation efficiency. For a plate element the coefficients are respectively:

$$\tau_{plate \to cav} = \frac{2\beta\sigma}{2 + \beta\sigma} \qquad \textit{Eq. 22}$$

$$\tau_{cav \to plate} = \beta \, \frac{{c_{cav}}^2 \sigma}{{c_{cav}}^2 f h} \qquad \textit{Eq. 23}$$

Where β is the relation of the plate´s and cavity acoustic impedances

$$\beta = \frac{\rho_{cav} \cdot c_{cav}}{\rho_{plate} \cdot c_{plate}} \qquad \text{Eq. 24}$$

With c speed of sound and ρ respectively the density of the plate and the one of the cavity, f is the frequency while h is the plate thickness.

The transmission coefficient matrix $[T]$, which result in a non-symmetric matrix is expressed as:

$$[T] = \begin{bmatrix} 1 - \tau_{plate \to cav} & \tau_{cav \to plate} \\ \tau_{plate \to cav} & 1 - \tau_{cav \to plate} \end{bmatrix} \qquad \text{Eq. 25}$$

The reflection coefficients, means of how much of the wave is reflected in the discontinuity, can be evaluated as a function of the transmission coefficients, as:

$$\rho_{plate \to plate} = 1 - \tau_{plate \to cav} \qquad \text{Eq. 26}$$

$$\rho_{cav \to cav} = 1 - \tau_{cav \to plate} \qquad \text{Eq. 27}$$

For what concern the radiation efficiency, this one can be expressed as:

$$\sigma = \frac{P_{rad}}{\rho_{cav} \cdot c_{cav} \cdot S \cdot \overline{\overline{v_{eff}}^2}} \qquad \text{Eq. 28}$$

With P_{rad} is the plate radiated power, S the radiating surface and $\overline{v_{eff}^2}$ is the mean of the time and space averaged squared effective particle velocity.

Chapter 2

2.1 Model set up

Aim of the work is to correlate and optimize the models, based on experimental data already collected, with the results obtained from the simulations. In order to do that, at first a modal analysis has been run, obtaining the modes and relative frequencies for all the models, then the results have been compared through the NVH solver. The process and results obtain in this step will be present in next chapter, including all the results.

In this chapter the set-up of the models will be explained, including pictures of the specific models, for the FE structures and the EFEM built up will be explained as well.

2.1.1 Set up of FE structure models

In this chapter will be described the set-up of the simulations for all the models employed.

First of all, it is worth of mention that before setting up the steps for simulation in the software, as already mentioned in 1.5.1, a preliminary work has to be done on the model. A check on the geometry has to be provided, at first with the command in the panel “Geom” in Hypermesh, that evidences the type of lines present in the model. In this section, there is the possibility to check how the geometry of the part has been modelled, in particular which are the construction lines and how they are connected. In the window are displayed mainly green, yellow and red lines. As a first step the yellow and red lines have to be converted into green ones. If they are present because of an edge, the edge has to be toggled, and if the lines are not continuous but detached, they have to be joined. Similarly, it happens with the yellow lines, Hypermesh allows anyway to work on the part even if they are present, but it is better to clean all the geometry anyway. As a second step, before applying the meshing conditions, the geometry has to be cleaned of all the unnecessary lines, but only the ones that don´t affect the overall geometry. This procedure has to be applied carefully to all the lines, and major attention has to be provided where two lines are pretty close. As a general rule, it can be said that, if part of the model presents a round edge (for example in the proximity of a hole), the round part has to remain both before and after the meshing. Another check that can be realized is the one to control if free edges are present. Sometimes can happen that the lines (yellow or red) referred to those edges are not quite visible, and thus this command is helpful in that.

For what concern the meshes, after deciding the dimension that is needed, it can be applied. For all the models that will be presented in this chapter, the interactive command has been used, instead of the automatic one. Both two are present in the section “2D, automesh”. The interactive command allows choosing surface-by-surface, and to decide how many elements are present on each side of the surface. To provide a better aspect to the quality mesh and have more precise results, the “only quads” has been chosen when meshing. Of course, when not possible, some trias elements are present. The last but not least step, before starting the tetramesh (3D meshes), is the quality check, also available in the “2D, quality index”. In this section, after setting the properties of the meshes, including values for the Jacobian, angles etc, the meshes that do not fulfil those requirements are displayed. By means of some clean-up tools, they can be deleted or partly changed. Only after all the meshes fulfil the requirements, the tetramesh can be performed. The tetramesh command starts meshing from the 2D and converts them into 3D ones. This means that the CQUAD and TRIA elements are converted into the PYRA and or HEXA meshes. (They have been already discussed in 1.5.1).

For all the model’s simulations, a modal analysis has been carried out. The load collector chosen is the EIGRL card image, with range of frequency of interest set up: from 450 Hz up to 2500Hz. In the load step, instead, the METHOD(STRUCT) is chosen. The analysis gives then in output all the modes present in the range of interest, even including the eigenvalues related to all of them.

2.1.2 Plastic cross member

As depicted in figure, the plastic cross member presents quite a complex geometry. Before meshing it, the part has been cleaned from all the unnecessary lines, in particular near the holes on the corners, to allow a more precise mesh. Extra attention has been paid to the small round edges and holes present for the coupling with the two elastic bushings.

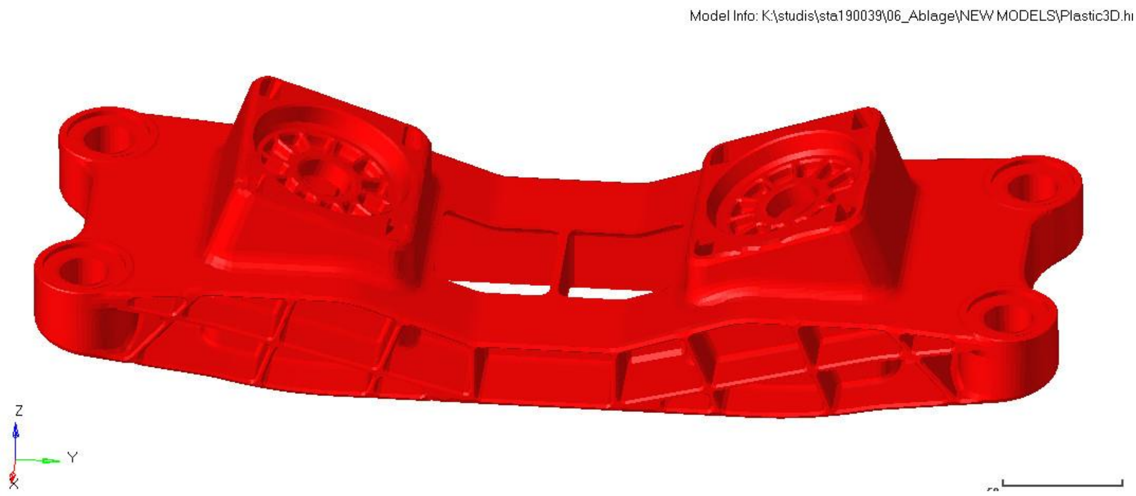

Figure 8. Plastic cross member model

The plastic employed is an Akromid.

The part is meshed firstly with 2D meshes of size 2mm and then it has been meshed into tetramesh, 3D elements, and results with:

- 235766 nodes
- 1046683 elements

After checking the conformity of the meshes, the modal analysis has been carried out. For the plastic cross member, the following modes have been found:

mode	f
1	738,011 Hz
2	865,244 Hz
3	1266,888 Hz
4	1993,413 Hz
5	2090,881 Hz

Table 1: Frequency modes for Plastic cross member

2.1.3 Aluminium cross member

The Aluminium cross member has a geometry similar to that one of the plastic one.

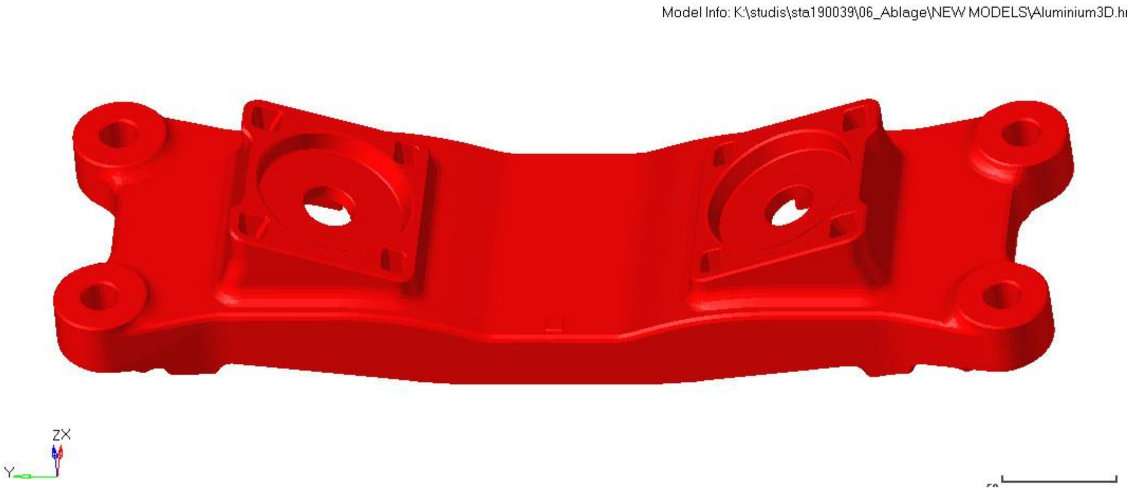

Figure 9. Aluminium cross member model

Analogously with the first plate, it has been modelled with 2Dmeshes, and then they have been converted into tetramesh, resulting in:

- 213428 nodes
- 987389 elements

The modal analysis has found out more modes in this case and they are:

mode	f
1	551,460 Hz
2	876,476 Hz
3	1680,365 Hz
4	2229,044 Hz
5	2331,496 Hz
6	2394,315 Hz

Table 2: Frequency modes for Aluminium cross member

2.1.4 Steel cross member

The steel plate is the one that has the simplest geometry. Nonetheless, it is composed of two different parts joined together.: physically speaking, the coupling is done by means of welding.

By simulating it, the coupling has been modelled in three different ways, respectively RBE, RDE and Midsurfaces, in order to understand which one could be the best way to approximate the real model, have an estimation and compare the results. Of course, there are several parameters that, already said, affect the final results such as dimensions and properties of the meshes, as well as, like for this case, the connections used. In the following are present some images concerning the overall aspect of the steel cross member, while more details about connections are shown in the relative paragraph.

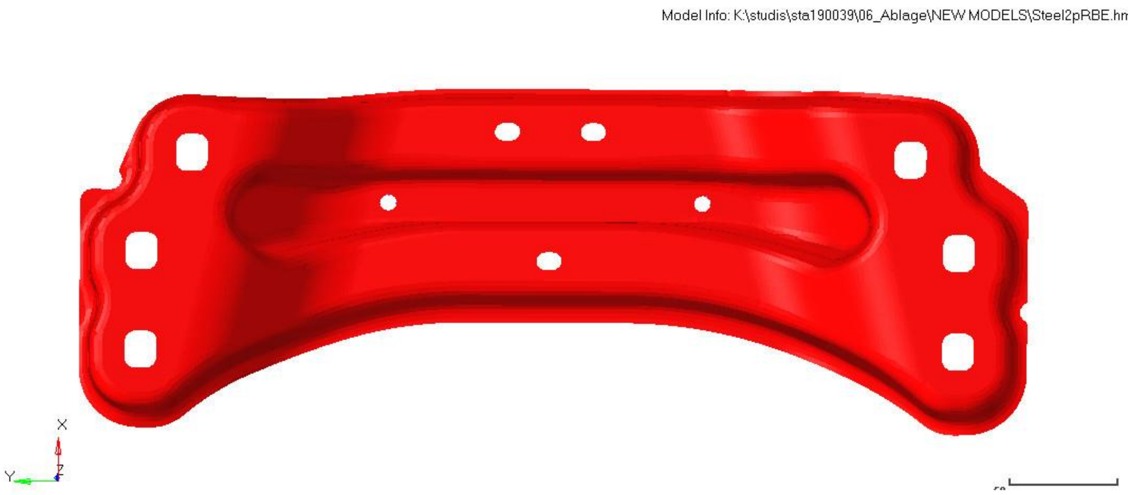

Figure 10. Front view of steel cross member

Figure 11. Partial rear view of steel cross member

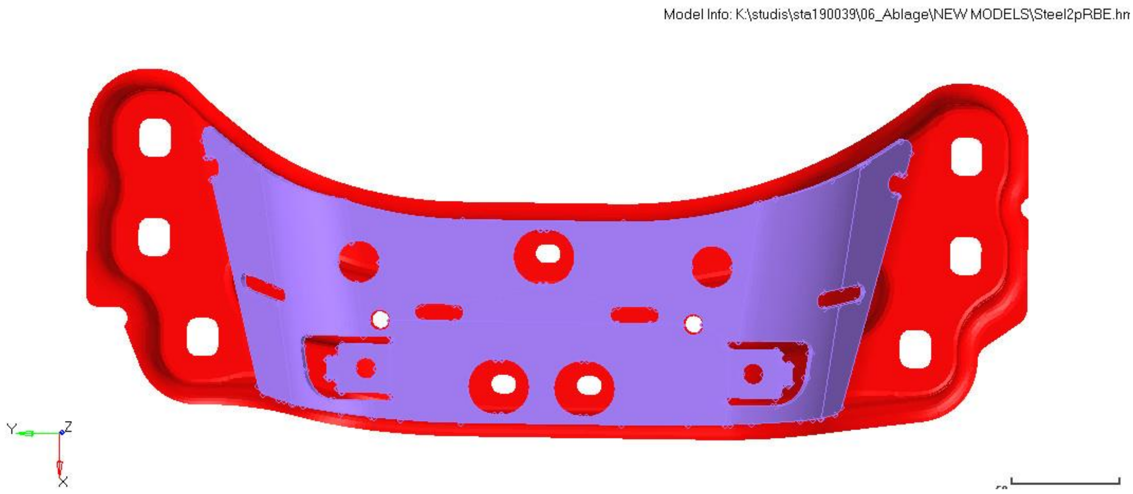

Figure 12. Complete rear view of steel cross member

2.1.5 Steel member modelled with RBE

The first type of connection employed, by joining the upper and bottom part of the steel cross member is the one with RBE connection. This one, the Rigid Body Element, is a connection between a central, master node (of an element) with some others. The central node dictates how the connected nodes move. Thus, the central node manager nodes and the connected nodes are the dependent nodes. This denotes the fact that the dependent nodes cannot move one relative to the others and form a rigid connection. This application is useful because leads to increase the stiffness of the component. In the following are represented the connections and their locations.

Figure 13. Detail of RBE connection on partial rear view of steel cross member

After meshing it with tetramesh elements, it results in:

- 169778 nodes
- 729923 elements

Also here, the modal analysis has been carried out. With respect to the modes got for the plastic and aluminium model, in this case we have more modes but geometry has changed too.

mode	f
1	755,423 Hz
2	767,237 Hz
3	1090,229 Hz
4	1249,637 Hz
5	1470,458 Hz
6	1793,363 Hz
7	1904,374 Hz
8	1934,377 Hz
9	1951,897 Hz
10	2035,626 Hz
11	2404,032 Hz
12	2482,441 Hz

Table 3: Frequency modes for steel cross member modelled with RBE

2.1.6 Steel member modelled with RDE

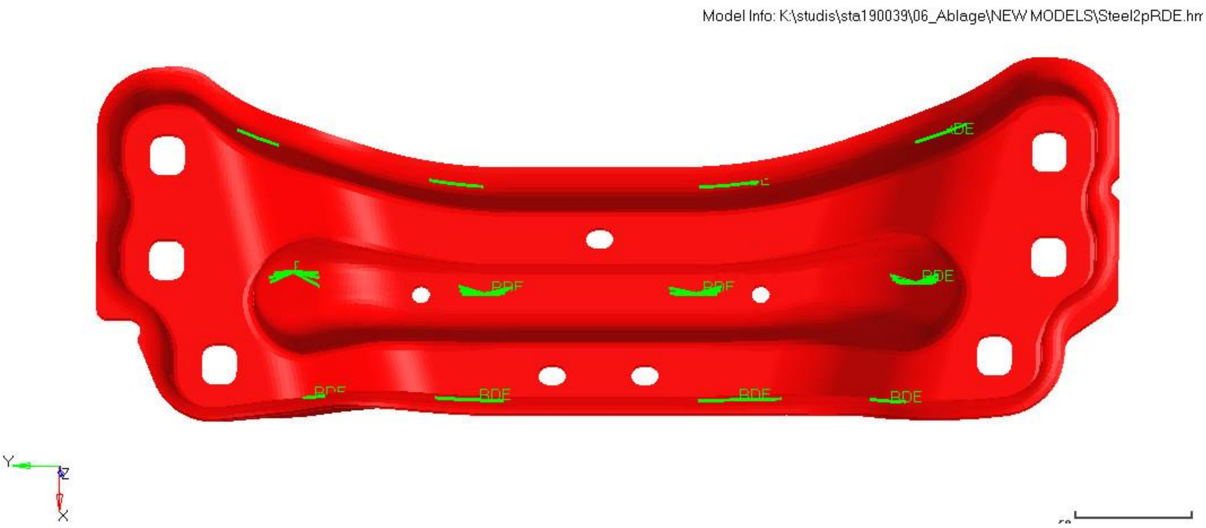

Figure 14. Detail of RDE connection on partial rear view of steel cross member

After meshing, the part results in:

- 133990 nodes
- 586173 elements

The number of modes, are closer to the case study with RBE connector.

mode	f
1	720,039 Hz
2	750,272 Hz
3	880,173 Hz
4	1014,301 Hz
5	1165,677 Hz
6	1243,019 Hz
7	1472,440 Hz
8	1725,174 Hz
9	1927,287 Hz
10	1945,113 Hz
11	2324,578 Hz
12	2432,886 Hz

Table 4: Frequency modes for steel cross member modelled with RDE

2.1.7 Steel member modelled with Midsurfaces

Mid surface is a meshing technique adopted in those cases in which components have a geometry thickness that is small when compared with the length span of the component. Thus, for this reason, the mid surface extraction is performed and thickness of the component is assigned to the elements through the properties of the component method.

Since the two parts of the steel cross member will result not attached after the mid surfacing, they have been joined with RBE3.

Figure 15. Front view of steel cross member modelled with Midsurfaces

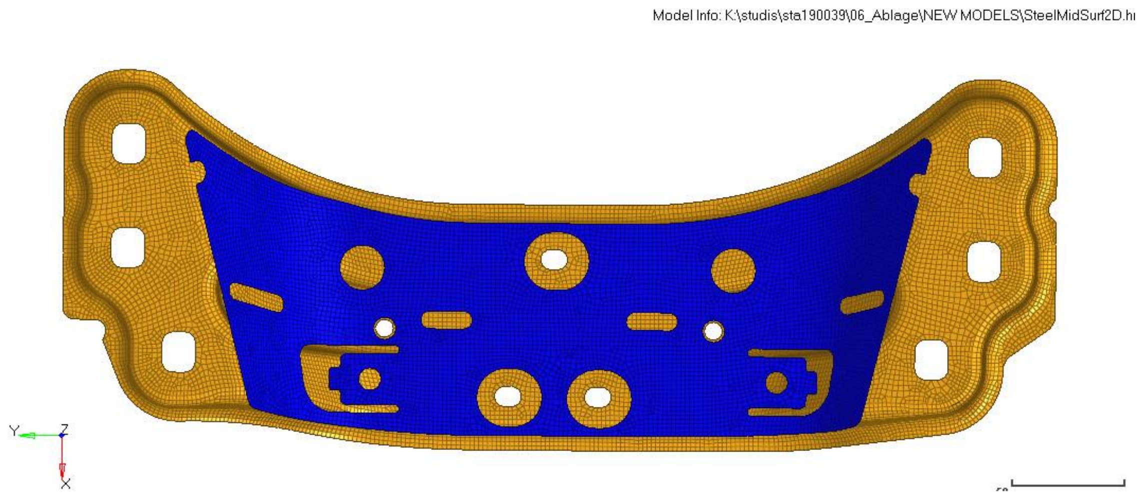

Figure 16. Rear view of steel cross member modelled with Midsurfaces

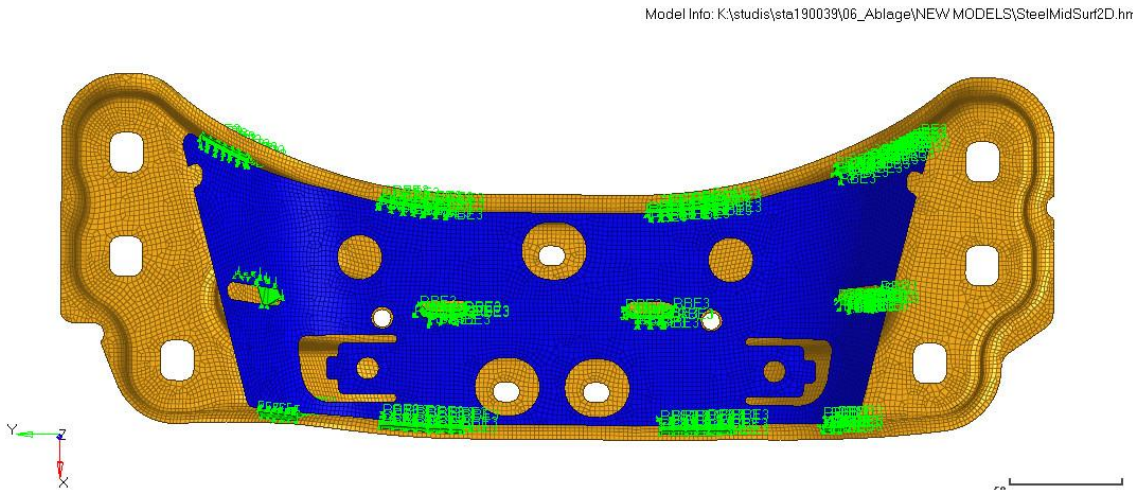

Figure 17. Detail of RDE connection on rear view of steel cross member modelled with Midsurfaces

After meshing the component, it results in:

- 31903 nodes
- 30980 elements

In this case study, differently than those ones modelled with RBE and RDE, the modal analysis comes out more modes and frequencies with respect to the previous ones. First of all, this has to be addressed to the fact that mid surfaces work with 2D elements instead of 3D, secondly, in this model are present both local and global modes. The ones to be interested on, then, will be less than the total 36, only the one in yellow

mode	f
1	523,005 Hz
2	574,563 Hz
3	616,304 Hz
4	630,303 Hz
5	653,950 Hz
6	753,073 Hz
7	765,061 Hz
8	905,704 Hz
9	1031,374 Hz
10	1238,960 Hz
11	1248,838 Hz
12	1265,525 Hz

13	1331,690 Hz
14	1380,543 Hz
15	1430,542 Hz
16	1500,185 Hz
17	1520,585 Hz
18	1544,501 Hz
19	1616,415 Hz
20	1668,913 Hz
21	1763,849 Hz
22	1783,190 Hz
23	1823,631 Hz
24	1864,408 Hz
25	1951,303 Hz
26	1974,544 Hz
27	2033,108 Hz
28	2088,651 Hz
29	2121,796 Hz
30	2214,180 Hz
31	2272,231 Hz
32	2328,013 Hz
33	2361,319 Hz
34	2370,848 Hz
35	2469,584 Hz
36	2492,079 Hz

Table 5: Frequency modes for steel cross member modelled with Midsurfaces

It is worth to underline the fact that the computation time for the three different case studies of the steel cross member hugely varies from case to case. In particular, the RDE is the fastest, around 16 mins, mid surfaces is in between (around 1h 20mins) while RBE is the slowest, 2h 25mins.

2.2 Set up of FE cavity models

The acoustic cavity meshing generates a fluid volume mesh that is used to evaluate which are the acoustic modes inside the air spaces of a structural model. It is mainly used in Noise, Vibration and Harshness analyses. In order to get the acoustic modes, a coupling has to be performed between the fluid volume and the part that has to be immerse in it. For the specific case used in this work, the structural parts have been put inside a cube, representing the chamber in which have been led the measurements. The coupling, depending on the type of software employed can be performed in different ways: by using NASTRAN, it can be done with the use of the Acoustic Cavity Mesh Panel, with the control card ACMODL, that directly couples the fluid with the structural part. Of course, even the properties of both fluid and structural components have to be specified. When creating the acoustic meshing for the cubic chamber, volume meshes are created for the fluid, i.e. the air that is contained in it, and in addition also the surface meshes, representing the border surfaces of the room.

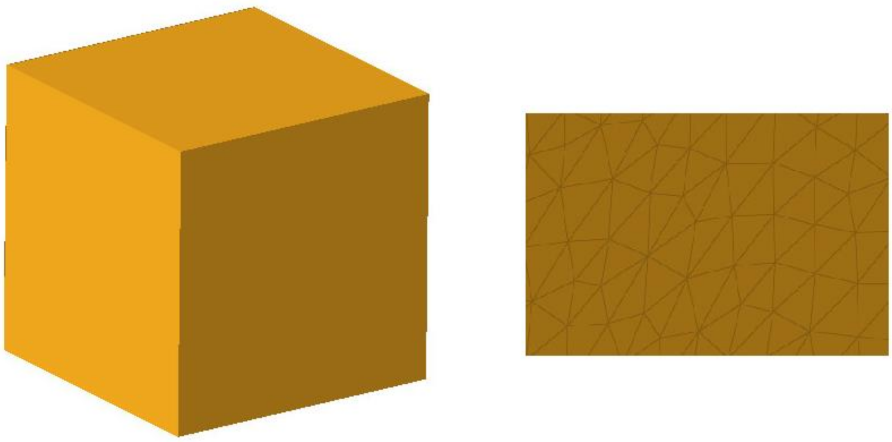

Figure 18. Cubic Chamber and surface mesh detail

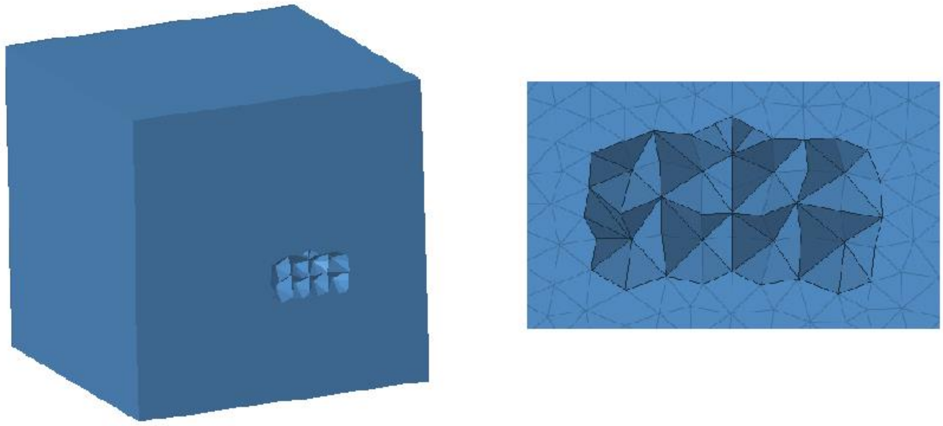

Figure 19. Fluid Volume in the chamber and tetramesh detail

In the card the property of the air is set: density and corresponding speed of sound. More than the modal analysis, other outputs can be specified, such as the pressure and the sound pressure level. In particular, the SPL computed on the surface areas of the simulated chamber is needed as input to perform the EFEM simulations.

2.2.1 Set up of EFEM models

By means of a standalone file, the FEM models used for the modal analysis have been converted into EFEM model. What the file substantially does is to create further connection between the elements. As already explained in subchapter 1.5.2, first goal that has to be reached in order to proceed with EFEM analysis is to add the nodes as well as the elements required to add the joint elements to fill the possible discontinuities present in the structure. This has to be done because the presence of a discontinuity means a gap in the energy density and this cannot be considered possible.
Thus, the FEM files have been exported in Nastran format (.bdf) and used by the file to create a new universal file with the complete list of new nodes, new elements and even the possible new joints elements too. The results of this procedure, with comparing the results obtained from the first models of FEM to EFEM will be presented in 3.4.

It is point out the fact that for the analysis and comparison of the steel model, only the case study that has got the best results in the MAC matrix evaluation has been used. This is done to save calculation time and to use directly the model that best approximates the real model.

3 Chapter 3

3.1 Model validation

In this chapter, the results obtained from the simulations will be analysed and compared with the ones coming from the experimental measurements, in particular an association between the values coming from the experimental data and the results obtained from the simulations in terms of MAC matrix evaluation will be displayed.

At first the validation will concern the FE models, focusing in particular on the results coming from modal analysis and their relative mode shapes and frequencies. Then an improvement on part of those results will be made and at the end the results coming from EFEM formulation will be presented.

3.2 Validation of FE models

For the validation of the FE models, the modes and frequencies coming from the modal analysis have been put into the NVH solver, so to create the MAC matrix. The Modal Assurance Criterion Analysis is a method used to determine the similarity of two mode shapes. This means that, if two mode shapes are equal, their correlation value will be 100%, thus 1 if considering the coefficient on the bar on the side. As a result, there will be one if the two mode shapes are highly correlated (equal), zero if they are not correlated at all and values in between for close mode shapes but not identical. The matrix will result in a double entry table, on one side there are the results of the correlation model, the one from simulation, while on the other side there are the results of the reference model, the one coming from measurements.
For the accuracy of the values between zero and one, the help of the animation modes from the simulations is helpful. It can be seen visually if the two mode shapes coincide or not, even if their correlation coefficient is not one.

3.2.1 Plastic model validation

For the plastic model case, both simulation and measurement have the same number of mode shapes.

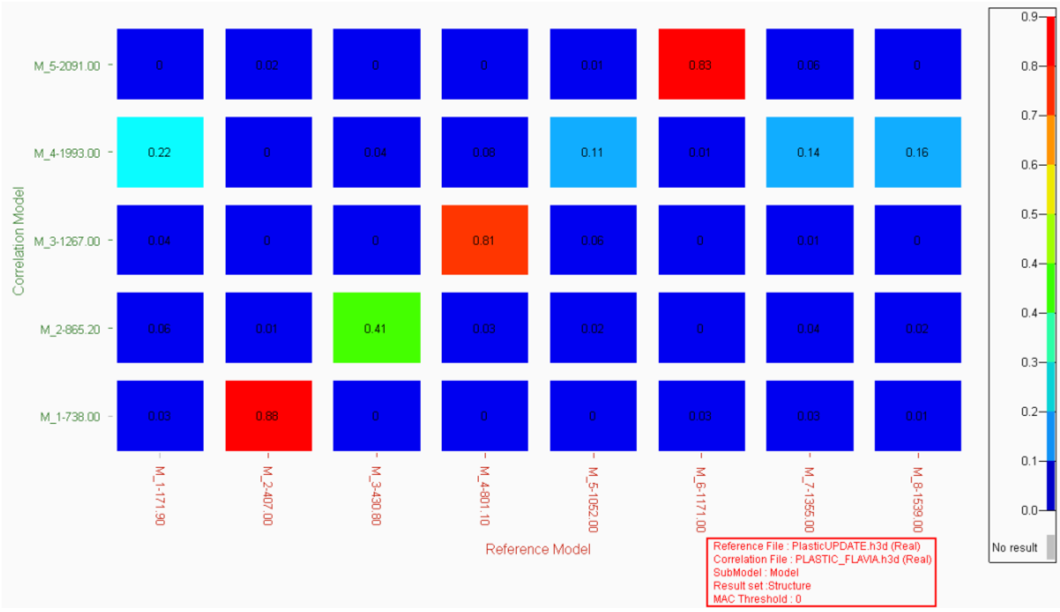

Figure 20. Plastic cross member MAC matrix

The most highly correlated mode shapes are the one in the red boxes: this means that the second mode shape of the reference model corresponds to the first one of the correlation, as well as the fourth of the reference corresponds to the third one of the correlation and the sixth one with the last one of the simulation. The fourth mode shape of the correlation model shows three different correspondences with the reference model, i.e. in the light blue boxes, with correlation factors between 0,14 and 0,22. In order to understand which one best correlates the fourth mode shape, the animation modes have been analysed.

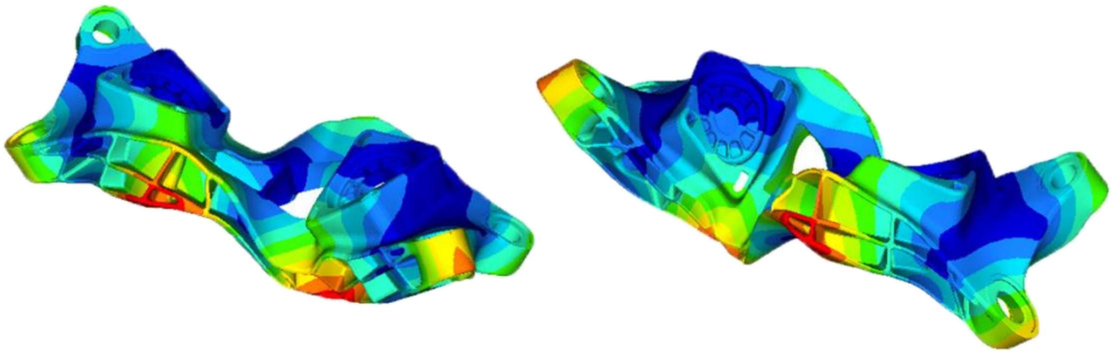

Figure 21. Mode shape 4 of plastic member correlation model

The first and last mode shape for the reference model, instead, have the following animation modes.

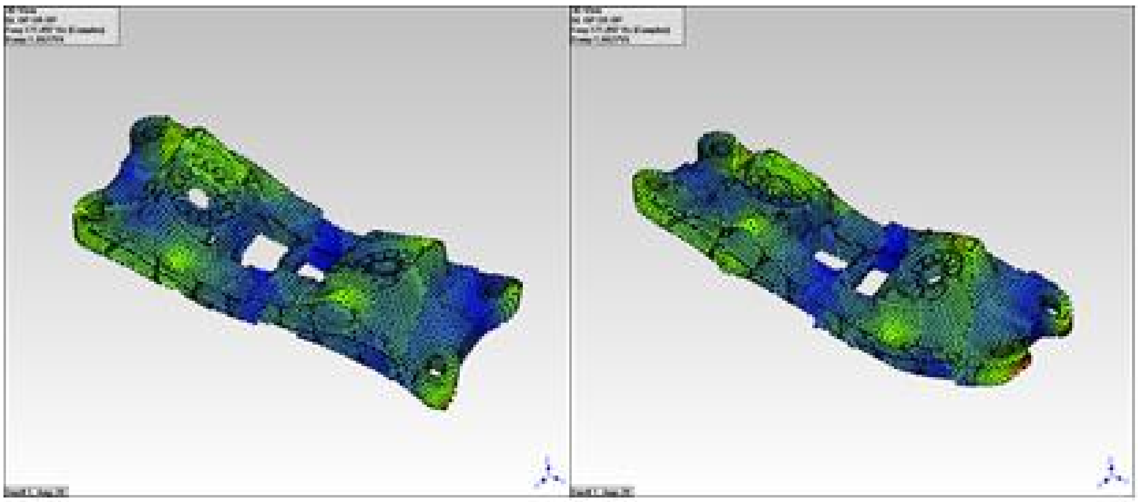

Figure 22. Mode shape 1 of plastic member reference model [HÜS18]

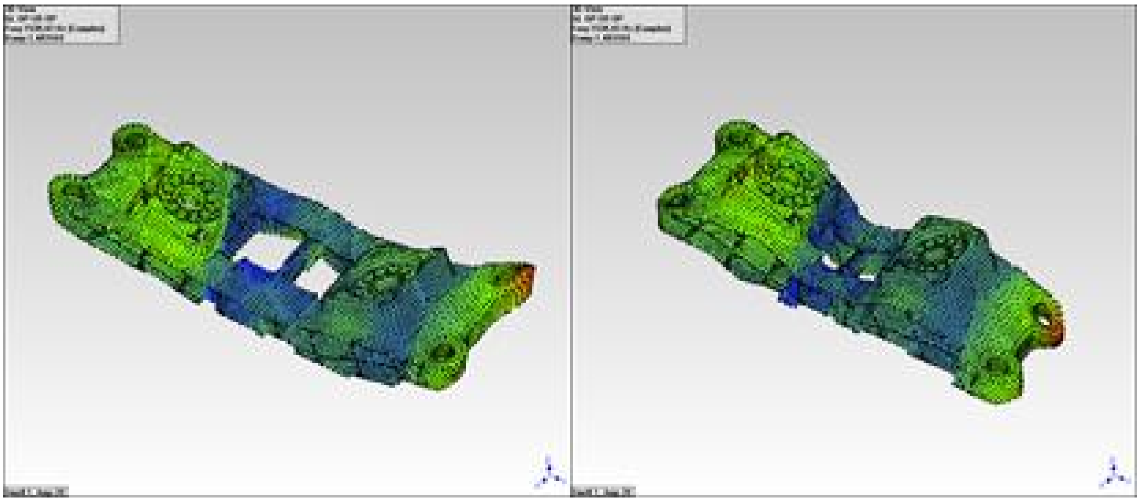

Figure 23. Mode shape 8 of plastic member reference model [HÜS18]

From the analysis of the animation modes the, it can be seen that the mode shape 4 obtained from the simulations, a torsion mode around y-axis, corresponds to the mode shape 1 from the measurement results, even if the correlation factor is not that high.

3.2.2 Aluminium model validation

The aluminium reference model, as depicted in the MAC matrix, presents more mode shapes than the correlation one and the last two have no correlation with it. For what concerns the other mode shapes, mode2 and mode4 of the reference correspond respectively with mode1 and mode3 of the correlation model.

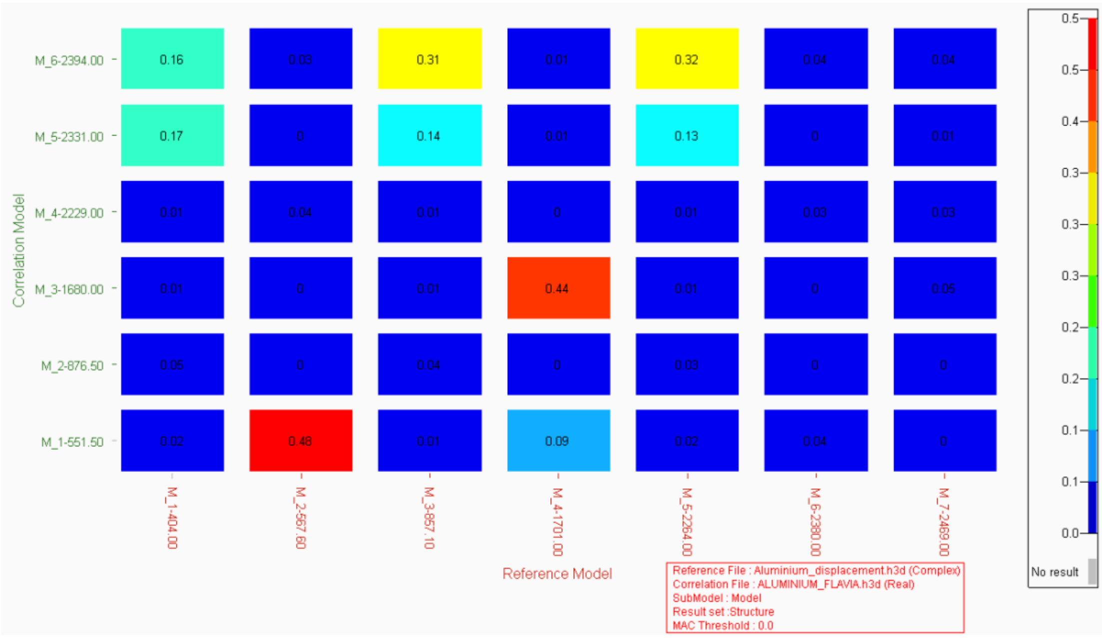

Figure 24. Aluminium cross member MAC matrix

The visualization of the animation modes, instead, is carried out for mode1, mode3 and mode5 of the reference with the mode5 and mode6 of the correlation model.

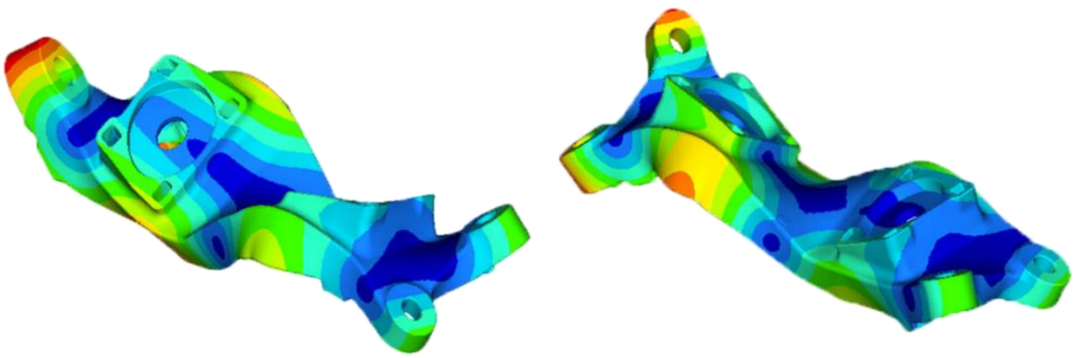

Figure 25. Mode shape 5 of Aluminium member correlation model

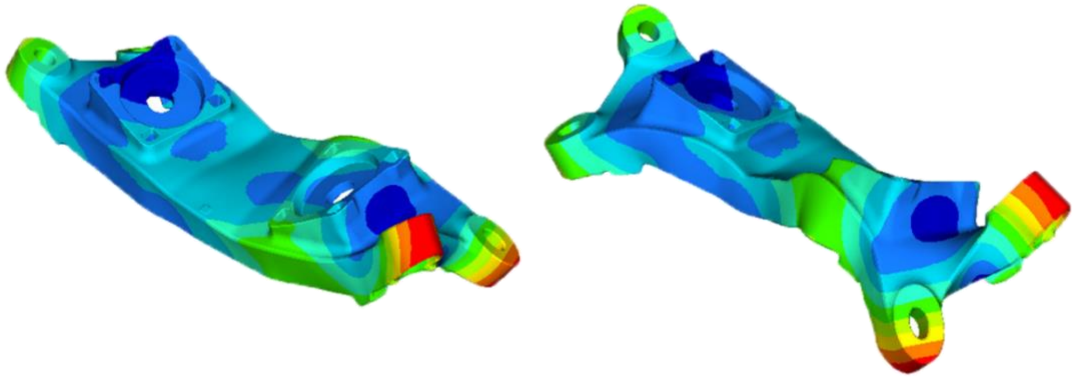

Figure 26. Mode shape 6 of Aluminium member correlation model

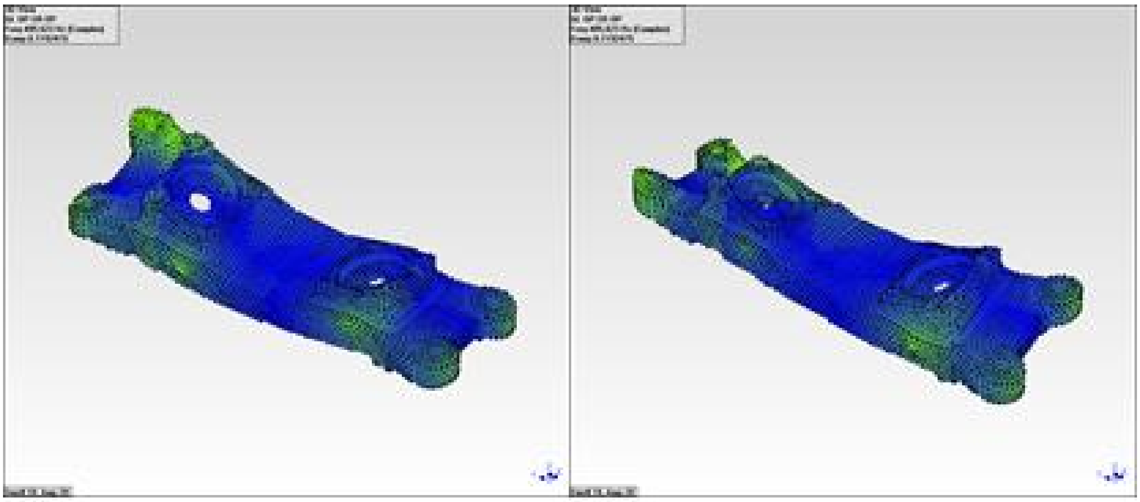

Figure 27. Mode shape 1 of Aluminium member reference model [HÜS18]

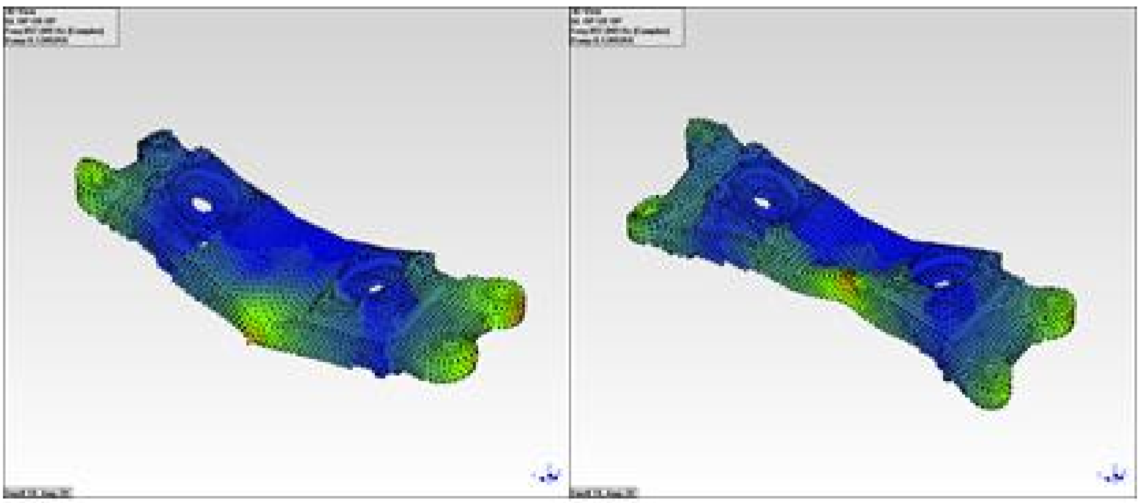

Figure 28. Mode shape 3 of Aluminium member reference model [HÜS18]

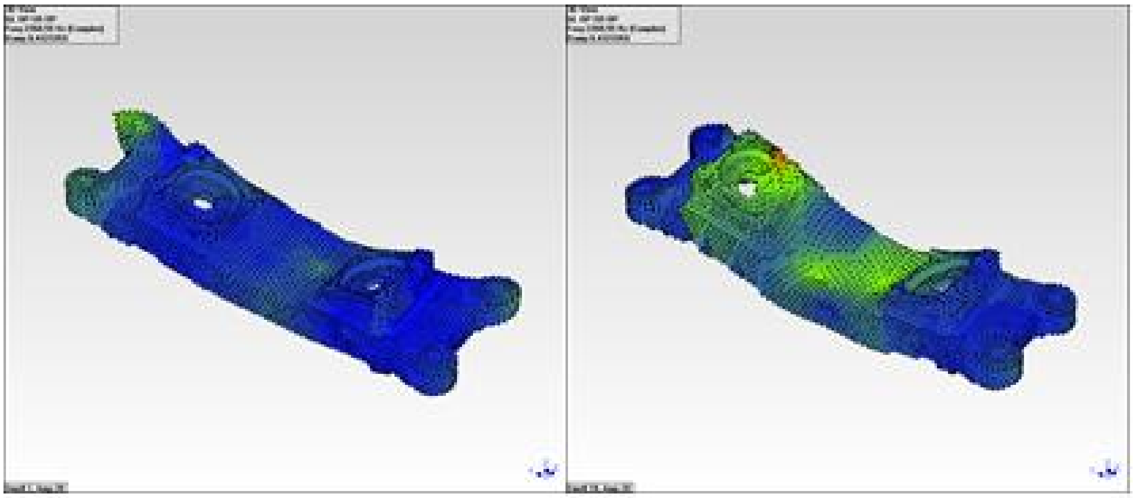

Figure 29. Mode shape 5 of Aluminium member reference model [HÜS18]

With the help of the animation modes, the mode shape 5 of the correlation model can be addressed to the first mode shape of the reference model, it is clear that corresponds to the same torsion mode around y-axis. On the other hand, the mode shape 6 is referred to mode shape 5 of the reference model, in which there is a combination of torsion and bending. Furthermore, the mode shape 3 resembles the last one of the correlation model, but has less correspondence than the mode shape 5 when looking at the animation modes. For the last two mode shapes of the reference model, they can be defined impossible to be correlated in no way to the simulated model. Their similarity can be augmented only if the MAC correlation will be improved.

3.2.3 Steel (RBE) model validation

The first case study of the steel cross member views almost double correlation model modes with respect to the reference one.

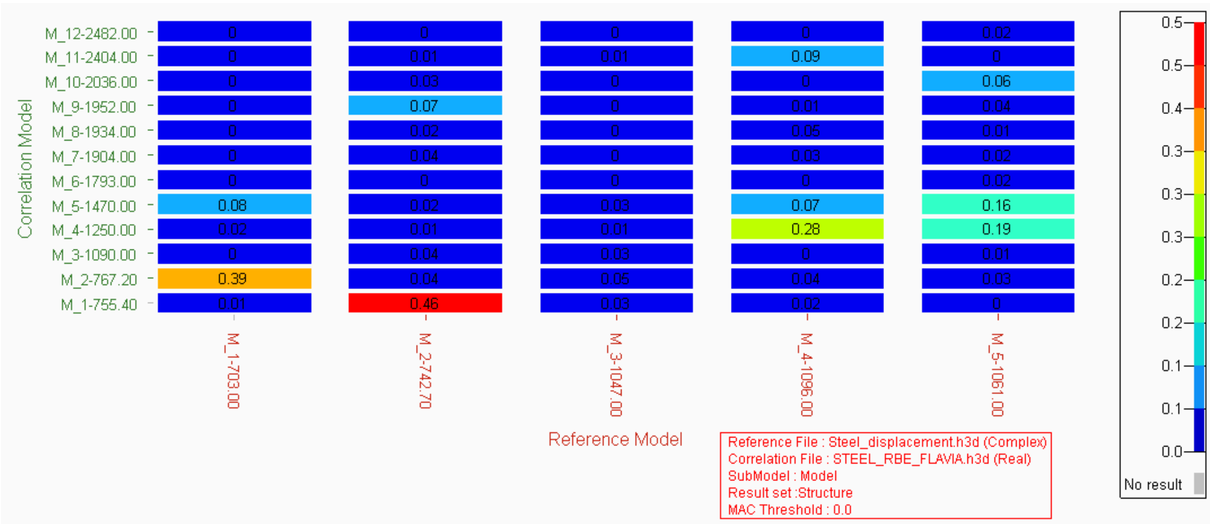

Figure 30. Steel cross member (modelled with RBE) MAC matrix

For sure, the mode2 of the reference corresponds to mode1 of the correlation, as well as mode1 of reference with mode2 of the correlation. For what concerns mode3 of the reference, it can be said not to be correlated since the coefficients of the MAC matrix are too low, at maximum 0.3 is displayed. For mode 4 and mode 5 the visualisation of the animation mode is considered, with mode4 and mode5 of the correlation model.

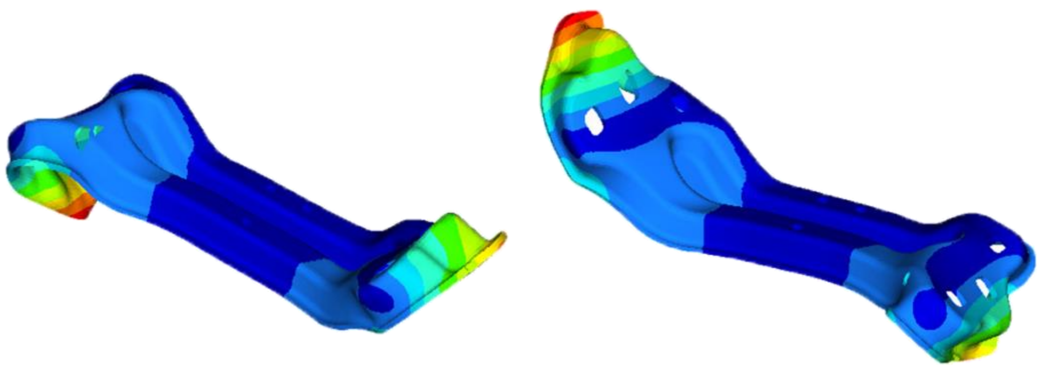

Figure 31. Mode shape 4 of steel member modelled with RBE

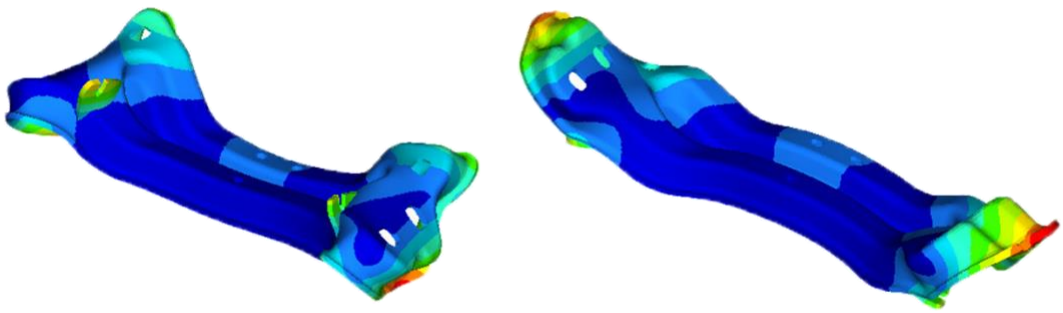

Figure 32. Mode shape 5 of steel member modelled with RBE

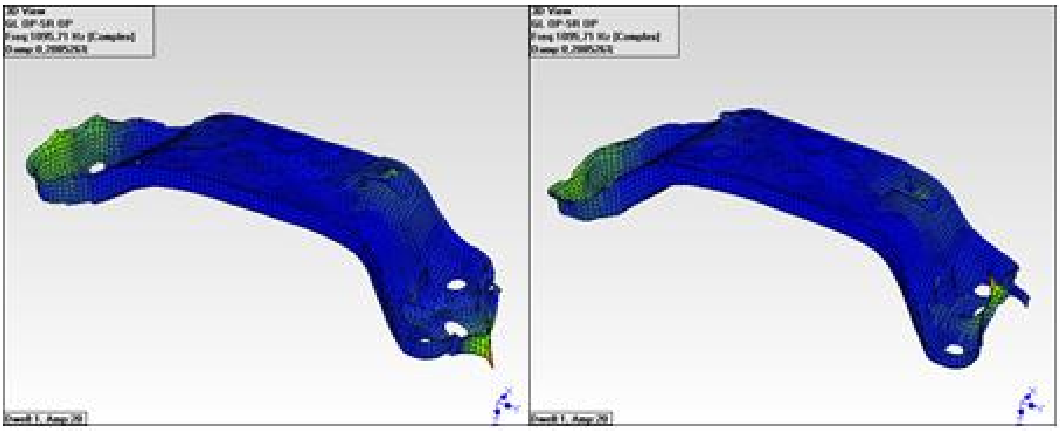

Figure 33. Mode shape 4 of steel member reference model [HÜS18]

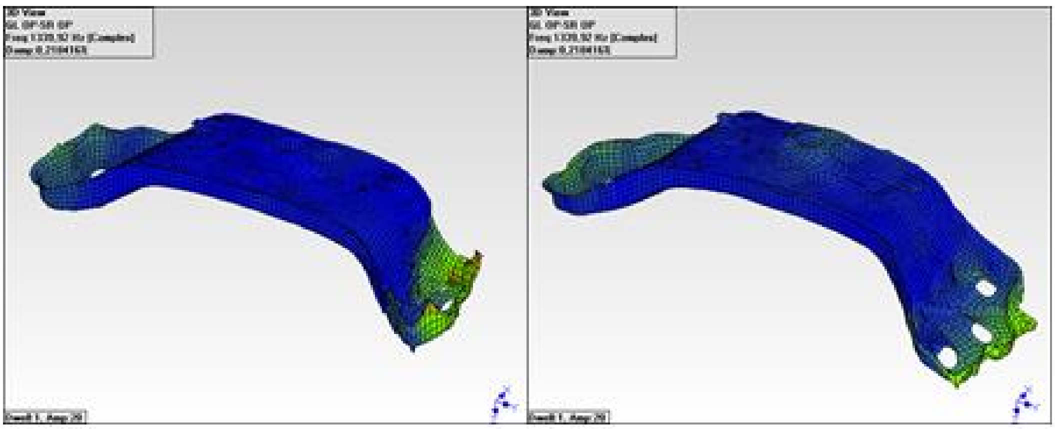

Figure 34. Mode shape 5 of steel member reference model [HÜS18]

From the animation view analysis, the mode shape 4 of the correlation model can be related to mode shape 4 of the reference mode, while both fifth modes can be correlated because from the animation views they appear to move in the same way, even if without the same values. Both are bending modes. Even in this case, values can be got better by improving the MAC matrix.

3.2.4 Steel (RDE) model validation

Similarly to the previous case study, the RDE modelled steel presents good correlation for the first two modes of reference-correlation model, while instead the mode3, mode4 and mode5 have to be checked with their relative animation modes.

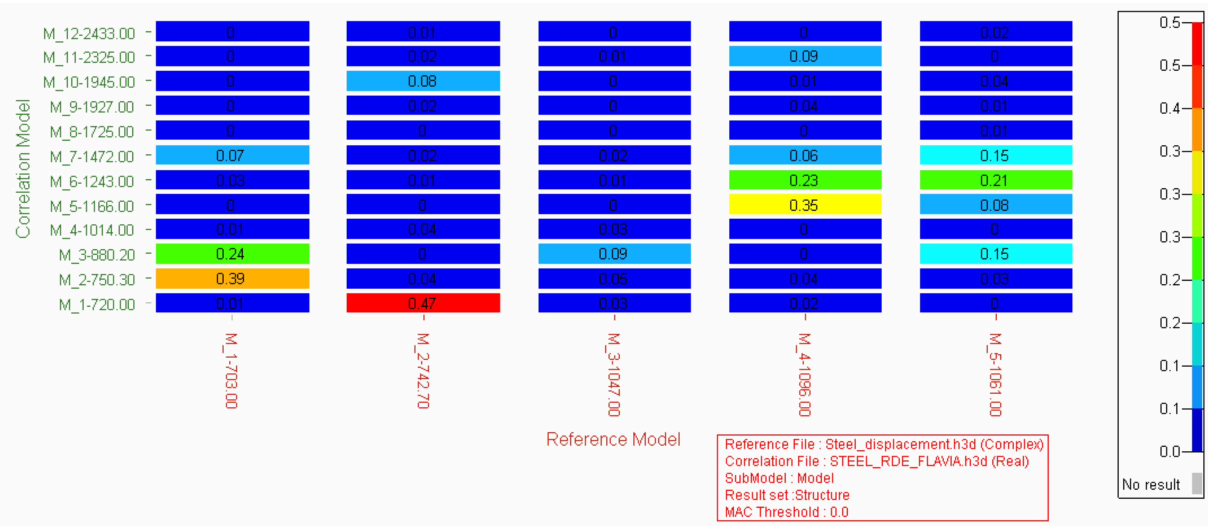

Figure 35. Steel cross member (modelled with RDE) MAC matrix

The animation modes of interest of the correlation model are:

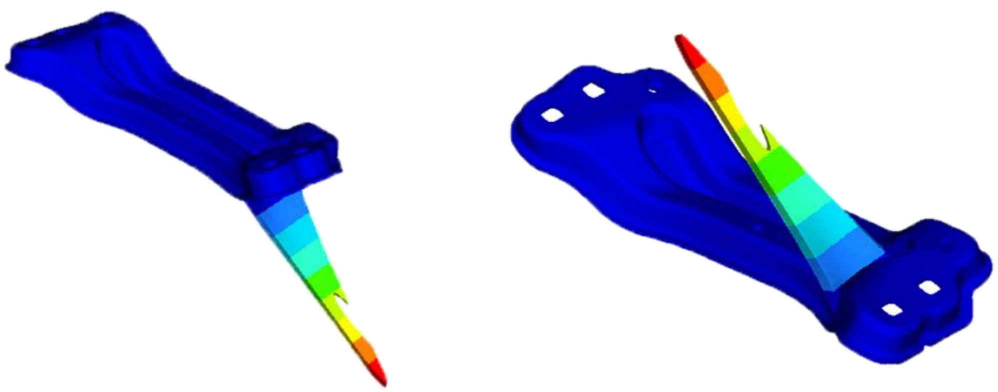

Figure 36. Mode shape 5 of steel member modelled with RDE

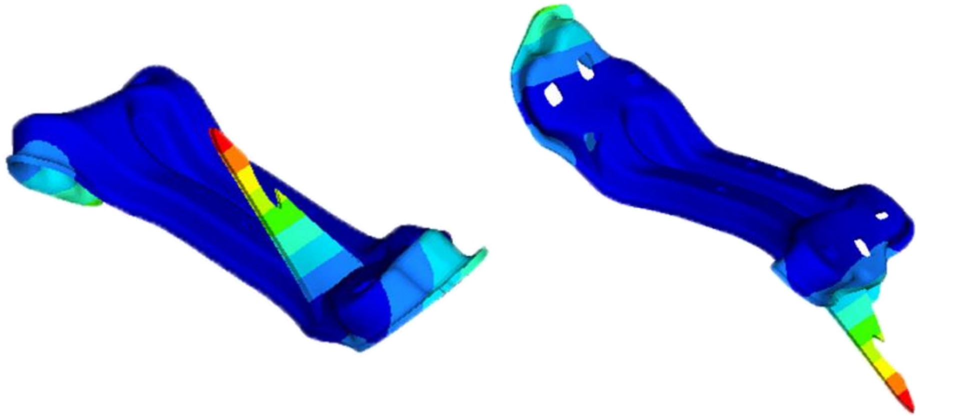

Figure 37. Mode shape 6 of steel member modelled with RDE

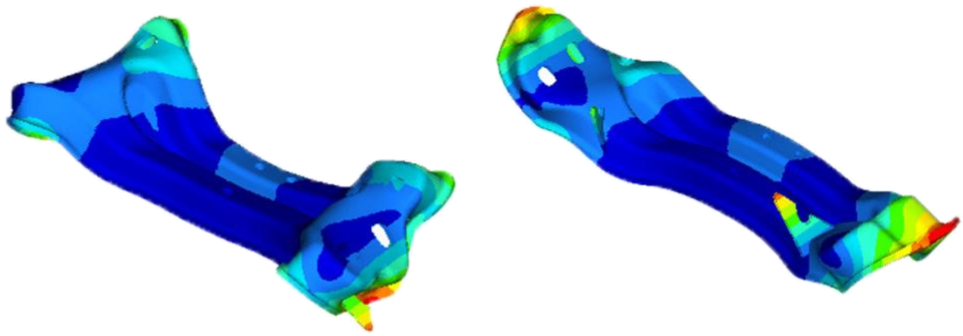

Figure 38. Mode shape 7 of steel member modelled with RDE

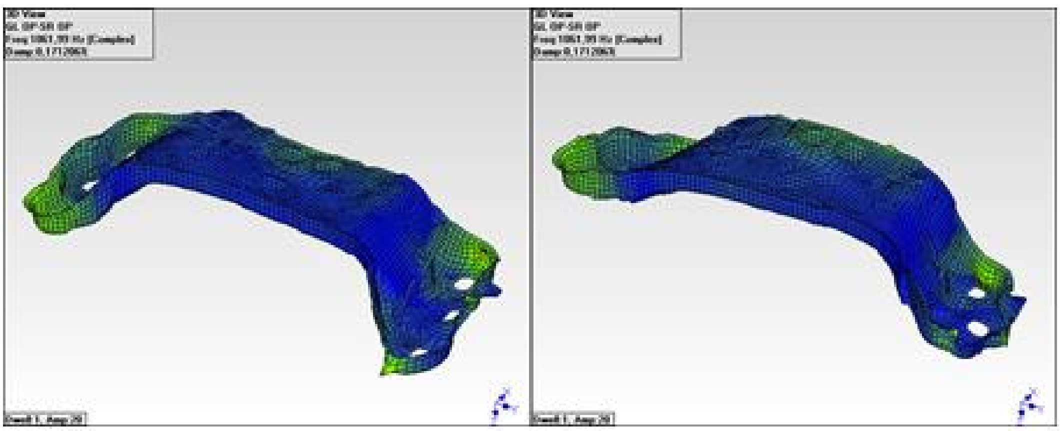

Figure 39. Mode shape 3 of steel member reference model [HÜS18]

In order to avoid redundancy, the mode shapes 4 and 5 for the reference model have not been reported again and can be found respectively in **Figure 33.** Mode shape 4 of steel member reference model [HÜS18] and **Figure 33.** Mode shape 4 of steel member reference model [HÜS18] For sure mode shape 4 of the reference model has quite good correlation with the mode shape 5 of the simulated model, the coefficient, in fact, is about 0.35. For the fifth mode shape of the reference model, it shows a relation with the mode shape 6 of the correlation model, even if the correlation coefficient is not that high but just about 0,21. The mode shapes three, for both the models have to be improved for sure, because the animation modes analysis shows a weak relationship as well as the MAC evaluation.

3.2.5 Steel (MidSurfaces) model validation

The Steel cross member modelled with Midsurfaces presents quite a lot of mode shapes, nonetheless only few of them are more interesting in this work since the local modes are not considered in favour of the global ones. In the MAC calculation, in fact, the local modes have been deleted in the evaluation. The fourth mode shape of the reference model finds a good correlation with the first mode shape of the correlation model, while the others have to be checked another time by means of the animation modes since the correlation coefficients are weak.

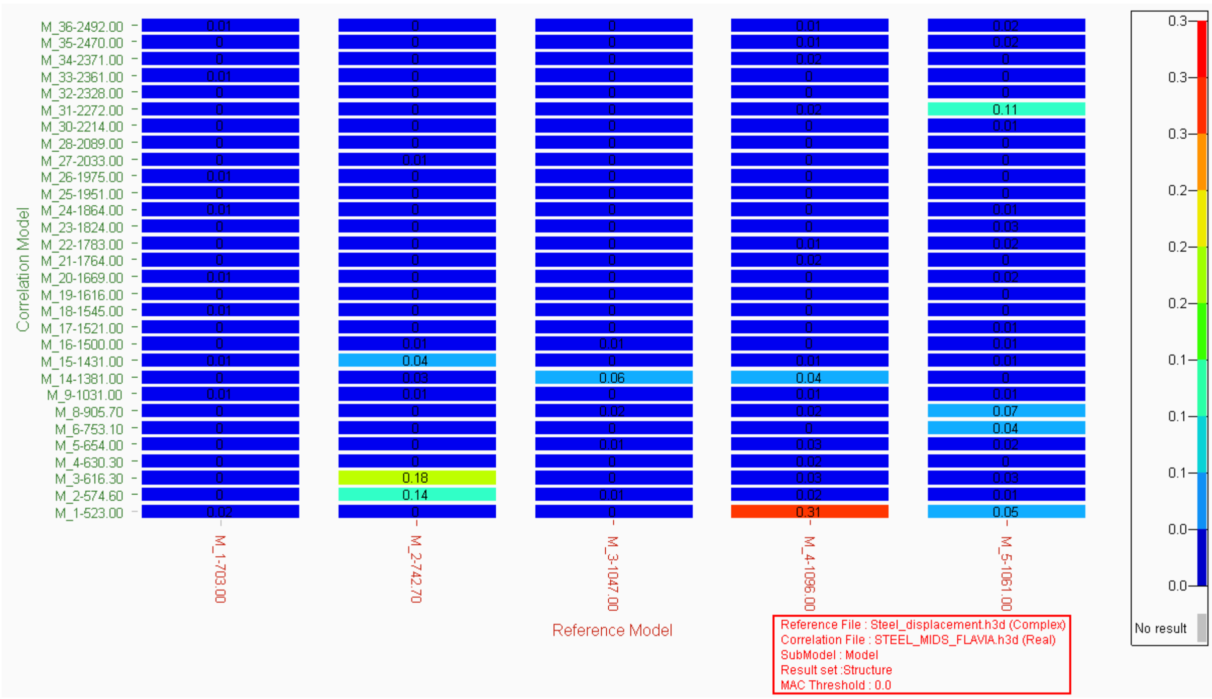

Figure 40. Steel cross member (modelled with Midsurfaces) MAC matrix

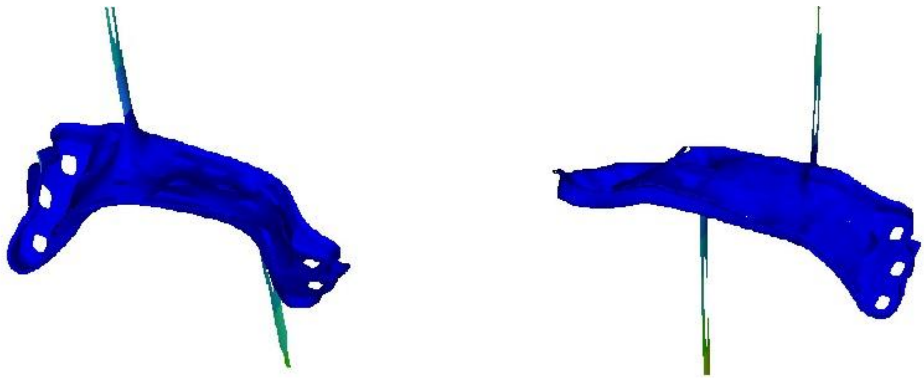

Figure 41. Mode shape 3 of steel member modelled with MidSurfaces

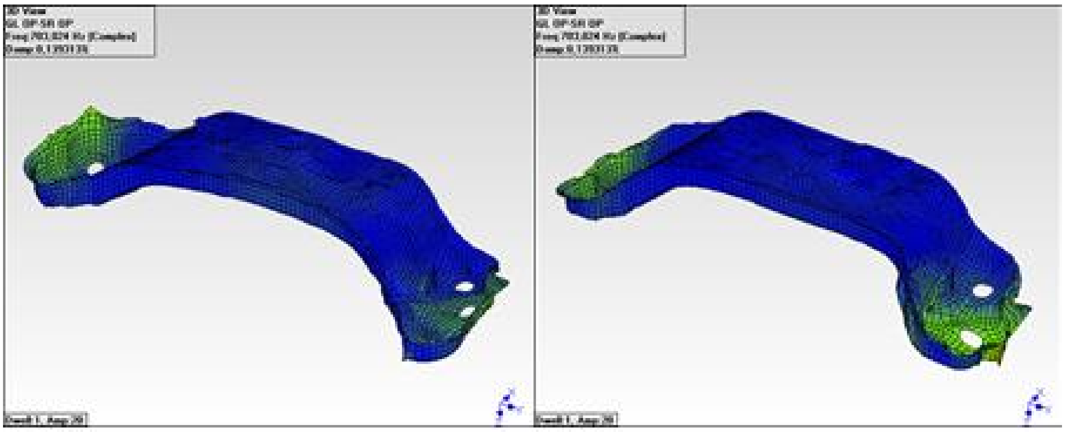

Figure 42. Mode shape 1 of steel member reference model [HÜS18]

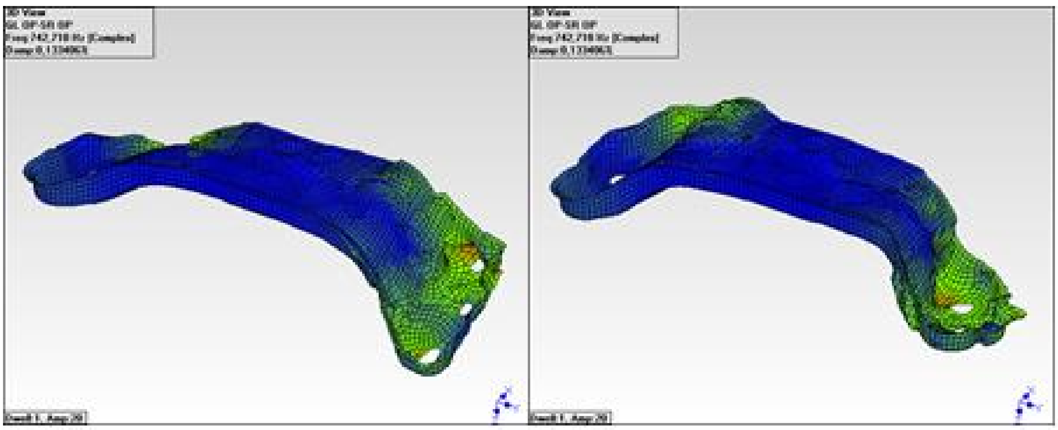

Figure 43. Mode shape 2 of steel member reference model [HÜS18]

For the Midsurfaces case study have been reported only the images of the still not outlined mode shapes figures. In this case study, since there are 2D meshes and not tetra ones, the frequency modes are much more than before. By the way, most of them can be left out and focus on the most important, which are the ones that shows a correlation in the matrix, even if the relationship is weak. Surely it can be stated that for the values of 0,31 and 0,18 coefficient of correlation the modes correspond, even checking the animation modes. The first mode of the reference model instead cannot be related to any of the simulated one because of zero correspondence. On the other hand, mode shapes 3 and 5 for the reference model have been analysed from the animation modes. The mode shape 3 and 5 for the reference model show anyway a weak correlation with the simulated model.

As a result, it can be asserted that the steel cross member modelled with the Midsurfaces has found the worse correlation with the reference model and, it has to be improved certainly in order to use it in the future.

3.3 MAC matrix improvement

As displayed in the different case studies, MAC matrix evaluates and correlates the measurement values with the simulated ones. Each model, thus steel, plastic and aluminium, has different points where accelerometers are put in order to measure the final displacements. Each model, in particular, is equipped with a different number of accelerometers, located in specific parts of the cross members. The nodes in which they have been located are respectively 15 for both the plastic and aluminium model while they are 48 for the steel cross member. The MAC matrix evaluation did so far, has been evaluated with all of them, for all the mode shapes. What could be interesting to analyse on the other hand, is the improvement the MAC correlation can be subjected to when considering only a small part of the total nodes.

The following pictures represent exactly where the measurement nodes for accelerometers are located in the cross members.

Figure 44. Real Plastic Model with upper measurement points [HÜS18]

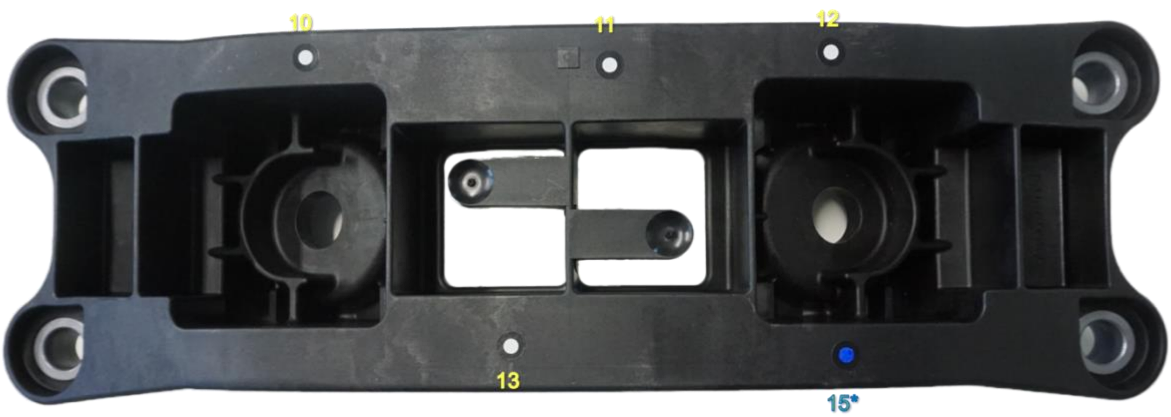

Figure 45. Real Plastic Model with bottom measurement points [HÜS18]

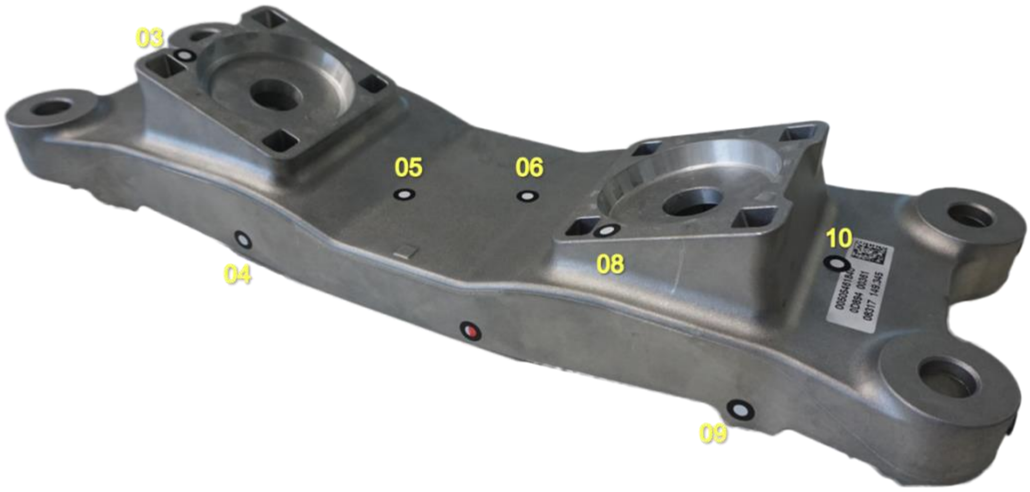

Figure 46. Real Aluminium Model with measurement points [HÜS18]

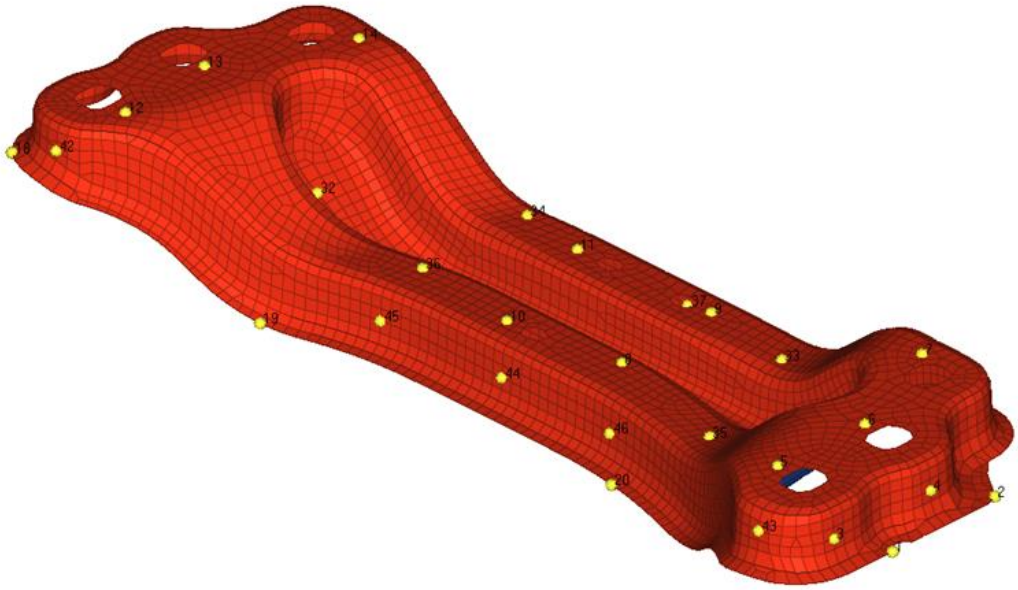

Figure 47. Steel model and measurement nodes for accelerometers [HÜS18]

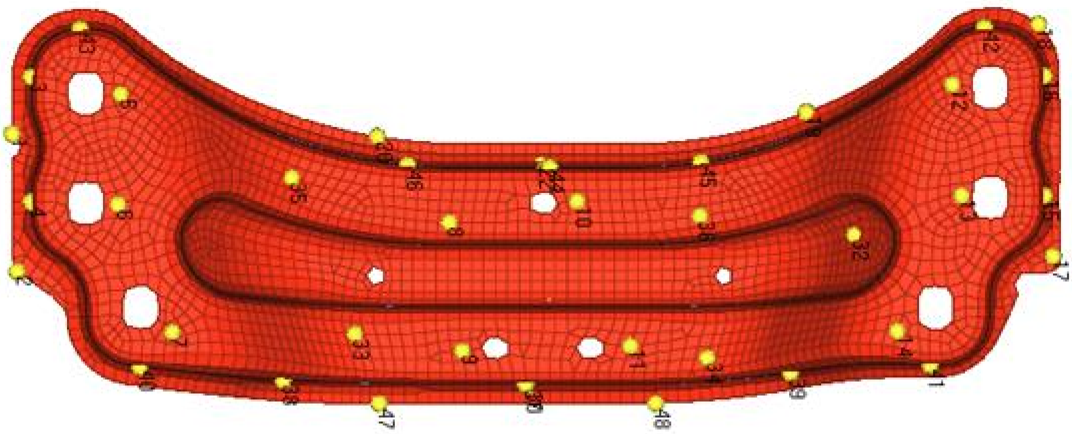

Figure 48. Steel model and measurement nodes for accelerometers, bottom view [HÜS18]

Practically, in order to improve the MAC matrix, since Hypermesh, doesn´t give the chance to exclude single nodes in the evaluation, a MATLAB script has been used for this purpose (reported in Appendix A). This one uses as input the shape table measurements and the simulation results. The first file is the one containing the measurements from the accelerometers, in term of displacement, while the second is always a shape table but for the simulated models. Then the script determines the natural frequencies and the eigenvectors and then computes the eigenvectors for all the modes. In the text there is the possibility to choose on which modes the investigation wants to be performed and even the ID of the nodes of interest. Only at the end, a picture of the MAC matrix is plotted, with a scale reference on the side with colours starting from blue for weak correlations up to red colours for stronger ones.

For the plastic model two different tries have been carried out: the first one only considering the nodes which are on the top of the cross member (from node 3 to node 9), while the second one only with the nodes at the bottom (from node 10 to node 15).

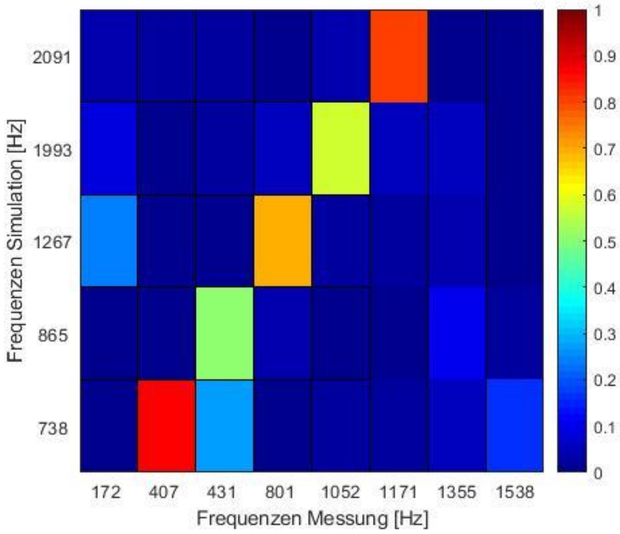

Figure 49. Plastic MAC improvement, upper nodes

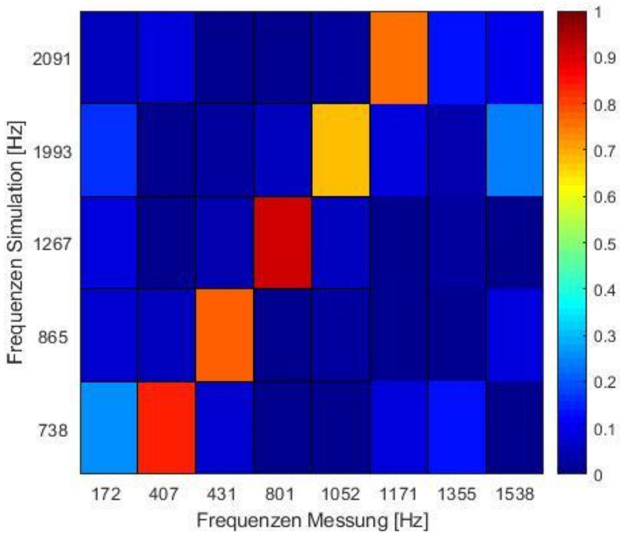

Figure 50. Plastic MAC improvement, bottom nodes

As it can be clearly seen, the second try only considering the bottom nodes has the best results. 4 out of 5 mode shapes have a really good correlation, with a factor between 80 and 100%. With respect to **Figure 20.** Plastic cross member MAC matrix, in which the last mode shape of the measured model had a weak correlation, now it has been increased effectively. It has passed, just because of the choice of the nodes from a correlation about 27% up to 80%. Just the first mode shape of the reference model remains little weak, but it has increased as well, from a value of 22% up to 35%.

For the Aluminium model also two tries have been performed: the first one only considering the upper nodes on the cross member (nodes 3,5,6,8,10) while the second one only considering those nodes on the sides (nodes 4,7,9,11,12,13).

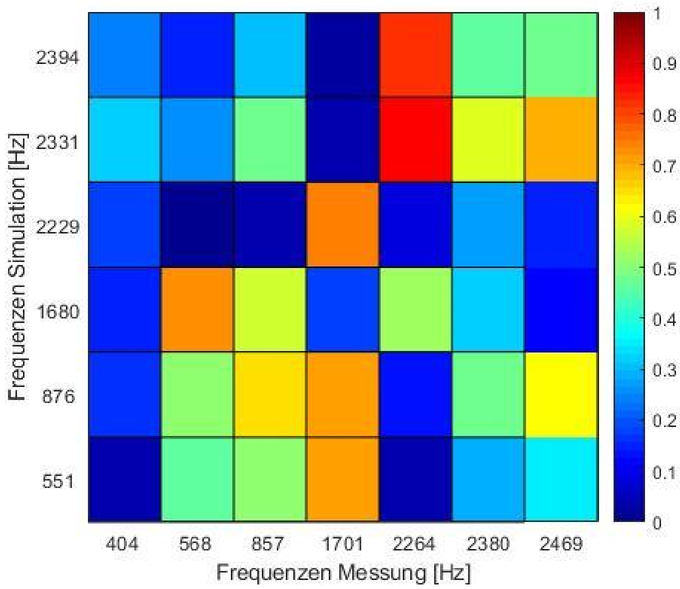

Figure 51. Aluminium MAC improvement, upper nodes

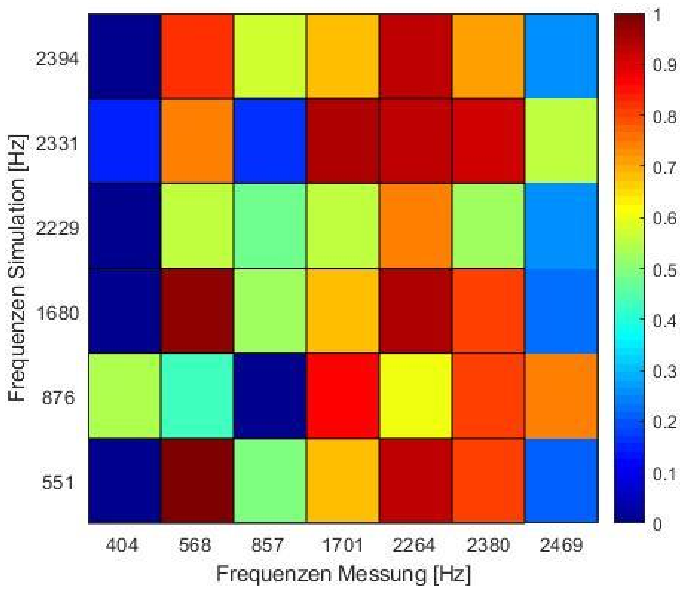

Figure 52. Aluminium MAC improvement, side nodes

The new MAC matrix coming from only considering the upper nodes shows an improvement with respect to the first MAC matrix obtained in **Figure 24.** Aluminium cross member MAC matrix. Apart from the first mode shape of the reference model, all the other mode shapes at different frequencies show a good correlation factor, roughly between 60% and 90%, while before the maximum correlation was around 48%. The case more interesting is the one considering only the side nodes, in which for almost all the frequencies we have the maximum correlation.

For the steel model, the same attempts have been performed, since the model is always the same and the measurements values are as well, what really changes is just the simulation modelling. In particular, the nodes that have shown better improvement results have led to five different attempts. The nodes only on the upper part of the cross member (nodes 8,9,10,11,33,34,35,36,37), the one at the bottom (nodes from 21 to 31), and then three others containing nodes on side, on the lateral sides (nodes 5,6,7,12,13,14) and the ones on both longitudinal sides (nodes 19,20,44,45,46 and nodes 37,38,39,47,48).

For sake of simplicity and in order not to be too much dense with pictures, only for the first case study will be attached all the images for the five attempts, while for the remaining case studies only the best improvements in MAC matrix evaluation will be reported.

For the first steel member case study, the first MAC evaluation led **Figure 30.** Steel cross member (modelled with RBE) MAC matrix, where the RBE modelling where considered. By improving it with the MATLAB script, the following “new” MAC matrices have been found.

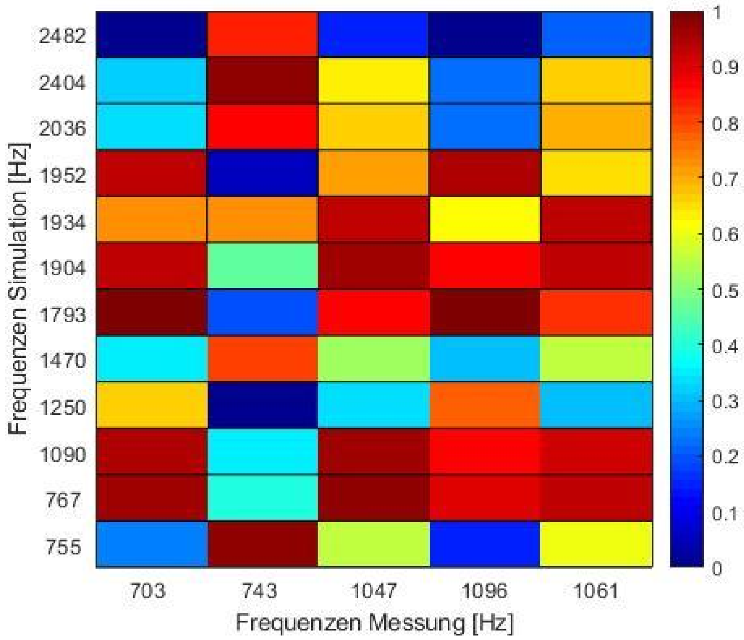

Figure 53. Steel MAC improvement, (RBEmodelling), lateral side nodes

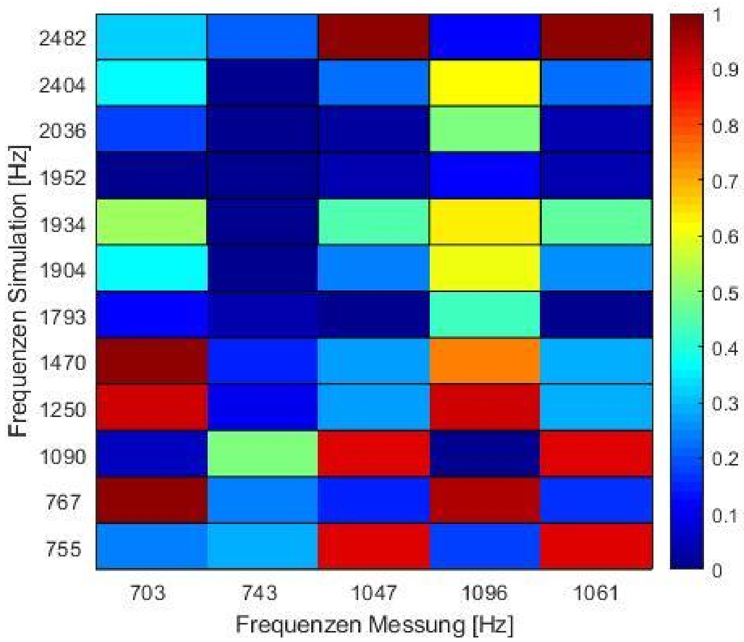

Figure 54. Steel MAC improvement, (RBEmodelling), upper plate nodes

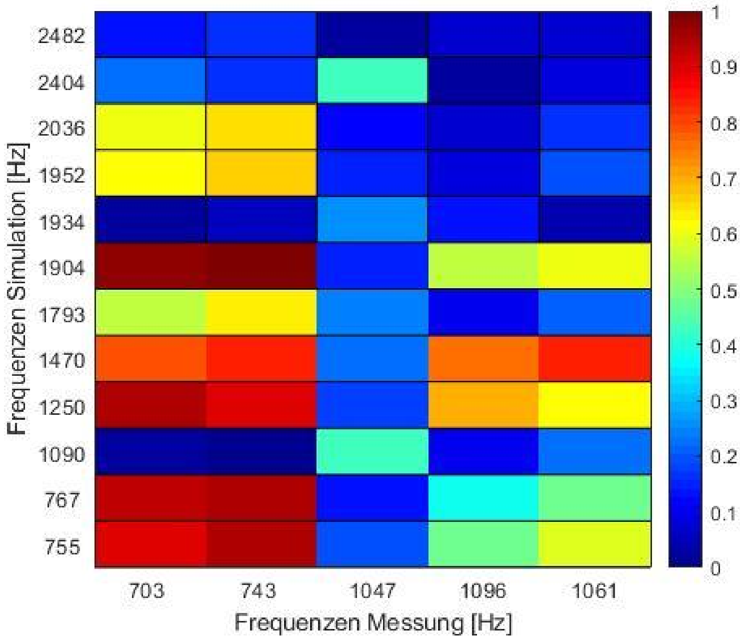

Figure 55. Steel MAC improvement, (RBEmodelling), 1st longitudinal side nodes

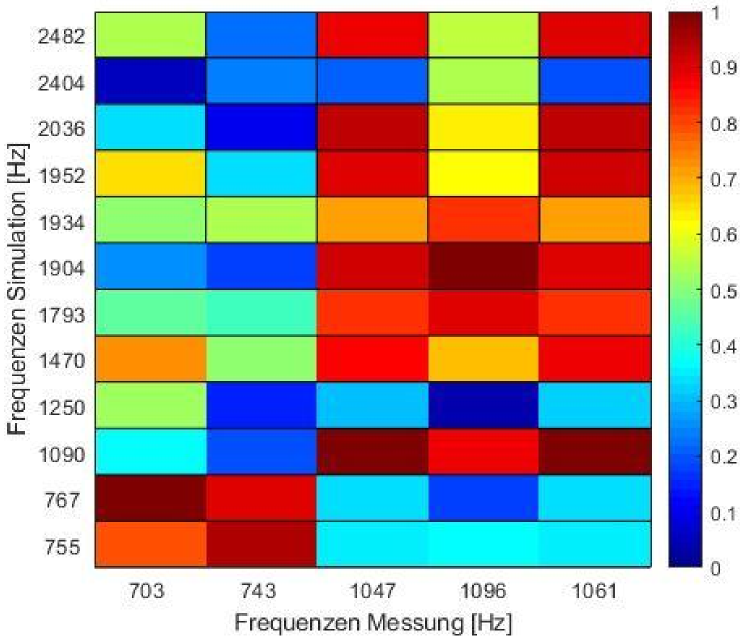

Figure 56. Steel MAC improvement, (RBEmodelling), 2nd longitudinal side nodes

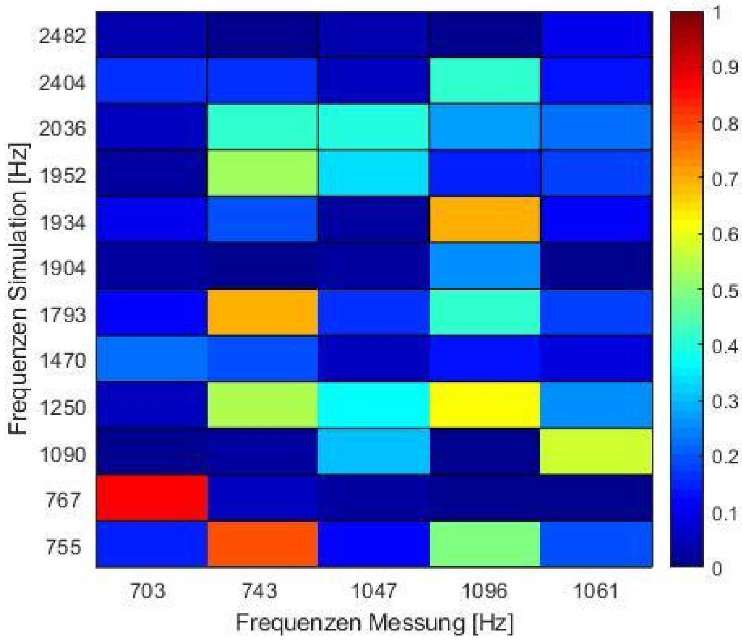

Figure 57. Steel MAC improvement, (RBEmodelling), bottom plate nodes

Apart from the last case, in which only the bottom nodes were taken into account and the improvement can be considered almost null, for all the other four cases, the refinement is clearly visible. For the cases in which just the nodes on the longitudinal sides were considered, the major change is visible or in the first two mode shapes or in the last three ones. The nodes in the upper part of the plate remark a good change if considering the first MAC matrix in **Figure 30.** Steel cross member (modelled with RBE) MAC matrix but the best results are shown if considering only lateral nodes in **Figure 53.** Steel MAC improvement, (RBEmodelling), lateral side nodes is a good sign of the improved correlation among the shape modes. For all the frequencies, there are at least three really good correspondences (in a range between 80% and 100%). In fact, for those frequencies that are closer, as 1047 and 1096, in the simulated model was experienced a combination of those two modes. In the improved MAC matrix, this fact is enhanced and their correlation factor values are high.

For the RDE case study, we have a good improvement among all different frequencies if considering only the nodes present on the lateral side (nodes 5,6,7,12,13,14).

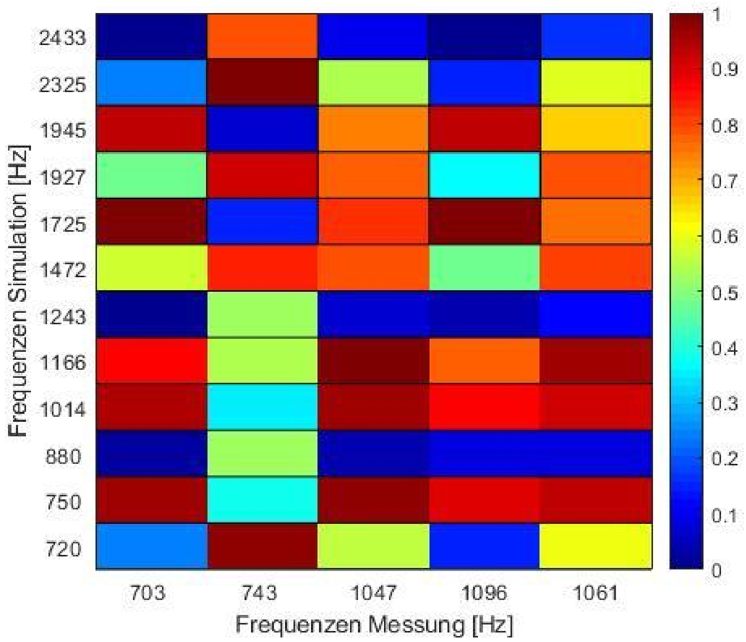

Figure 58. Steel MAC improvement, (RDEmodelling), lateral side nodes

The new calculated MAC matrix shows high correlation factors, from 0,8 up to 1, for almost all the frequencies. In particular, with respect to the previous evaluated matrix, in **Figure 35.** Steel cross member (modelled with RDE) MAC matrix, correspondences have increased mostly for the last frequencies of the simulated model and the last mode shape of the measured one.

Also for the MidSurfaces case study, only the best improvement in the MAC matrix will be reported.

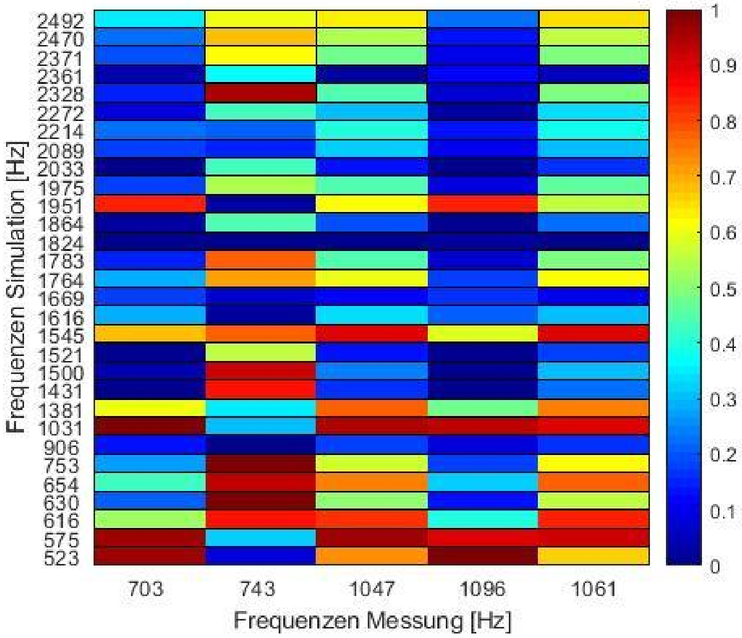

Figure 59. Steel MAC improvement, (MidSurf modelling), lateral side nodes

With respect to **Figure 40.** Steel cross member (modelled with Midsurfaces) MAC matrix, the fourth mode shape of the reference model now have a greater correlation, it passed from having a factor of 0,31 to a unitary value; the same happened even for the second mode, where correlation increased. Also the first mode, now, has a high correlation with the first two of the simulated one.

3.4 Validation of EFEM models

For the validation of the EFEM models the file coming as an output from the standalone file to convert FEM models, gave unexpected results.

The new files have to be check both for nodes and for elements, in order to investigate the joint elements added for the EFEM but, what results is that the number did not changed. To make quicker calculations and save some time, the plastic model and the aluminium model have been used with 2D meshes, while instead, for the steel cross member, the best-case study, which was represented by the RBE modelling was used.
Both before and after the creation of the file, the Plastic model results in:

-82659 nodes

-2465 CTRIA elements

-81456 CQUAD elements

For the Aluminium model, it results in:
-64887 nodes
-2805 CTRIA elements
-63504 CQUAD elements

The steel model, instead, since it was used the one with RBE modelling, and that one has been performed with 3D meshes, it will have:
-169728 nodes
-665802 CTETRA elements

It is worth of underlining the fact that, since the position of the nodes as well as the configuration of the elements can change for the EFEM formulation, a check on a random sample of 25 different nodes has been run out for all the three structures. It resulted to have the same number of nodes but for those analysed, the coordinates did not change at all. This means that, even if further and future investigation has to be performed to continue and conclude the EFEM analysis on the structures, the meshes done to evaluate the modal analysis, since the models were already enough complex, was pretty good.

Thesis Final Considerations

In this Thesis work the modal analysis and validation of EFEM models on three different cross members used to connect the suspension strut to the axle have been run: a plastic, an aluminium and a steel structure.

At first the models have been built up, studying the geometry, by simplifying it and only at the end meshing them. In order to make them as close as possible to the physical models, in particular for the steel cross member, since it presents weldings, different modelling techniques have been performed to see which model would have better described the real component. For all the three models a modal analysis has been achieved, mode shapes and resonance frequencies have been got to compare them with the results coming from the measurement results.

After getting modal analysis results and comparing them with the ones coming from the measurements, the MAC matrices have been built. The different mode shapes have been analysed and, when necessary, a distinction between local and global modes have been done.

At the end, in order to set up the model for the EFEM analysis, the acoustic cavity mesh has been built, studying the coupling that is necessary between the fluid that surrounds the structure and the structure itself. Only after that, a standalone file has been used to convert the FEM file into EFEM and see how the models have to be changed to perform the EFEM analysis. In particular, attention has been paid to the number of nodes, elements and possible joint elements added for the new analysis.

In this work the validation for the EFEM analysis has been carried out. As a future scope, there is the possibility to fully investigate the EFEM analysis by taking into account of what has been performed so far.

Even if the modal analysis carried out good values for what concerned the resonance frequencies and mode shapes, when comparing them with the experimental results, some values did not have the best correlation with each other. In the future the configuration of the meshes on the structure could be changed and only then, run again the modal analysis.

For the MAC matrix evaluation, which is a Modal Assurance Criterion, a first improvement has been done, considering in the calculation not all the measurement nodes where accelerometers have been put physically, but just few of those nodes. This has been done because if considering the different mode shapes and only few nodes for the accelerometer, the mode shapes measured vs. experimental one become closer. This method anyway does not affect any change in the results but sets the stage for future improvements.

The plastic cross member after the improvement showed good results, the aluminium structure had discrete results but for the steel model more work should be realised.

For what concern the EFEM analysis instead, a new improvement would be done investigating in more detail the joint elements that should be added to the structures in order to create a better, complex model for future calculations.

Appendix A

<u>Matlab Script for MAC matrix improvement:</u>

```
“clear all
close all
clc

%% Laden der Messdaten (Measurements)
% Laden der uff-Datei

[shapes_meas, Info, errmsg] = readuff('D:\Projekte\p190039_BMWi_Leichtfahr\06_Ablage\Toolbox\Externer Workshop\Korrelation\Shapes.unv');

% Bestimmung der Eigenfrequenzen
for j=1:numel(shapes_meas)
  freq_meas_total(j) = imag(shapes_meas{1,j}.eigVal)/(2*pi);
end

%% Laden der Simulationsergebnisse (Simulation)
% Ergebnisse liegen im pch-Format aus Hypermesh vor

% Laden der pch-Datei
fid_in = fopen('D:\Projekte\p190039_BMWi_Leichtfahr\06_Ablage\Toolbox\Externer Workshop\Korrelation\Stahl.pch');
% offnen der Datei
k = 1;
while ~feof(fid_in)
  pch_text{k,1} = fgets(fid_in); % Text in der k-ten Zeile der Datei
```

```
    k = k+1;
  end
  zeilen_moden = find(not(cellfun('isempty',strfind(pch_text,'$EIGENVALUE')))); % Nummern der Zeilen, in denen die Modennummern eingetragen sind
  anzahl_punkte = (numel(pch_text)-zeilen_moden(end))/2;

  % Bestimmung der Eigenfrequenzen und Eigenvektoren
  for j=1:numel(zeilen_moden)
    freq_temp = regexp(pch_text{zeilen_moden(j),1},'[\d.]+','match');
    freq_sim_total(j) = sqrt(str2double([freq_temp{1} 'e' freq_temp{2}]))/(2*pi); % [Hz] Alle Eigenfrequenzen der Simulation
    for k=1:anzahl_punkte
      shapes_temp = regexp(pch_text{zeilen_moden(j)+2*k-1,1},'[ +-][\d.]+','match');
      shapes_sim{1,1}.nodeNum(k,1) = str2double(shapes_temp{1}); % Knoten-ID
      shapes_sim{1,j}.r1(k) = str2double([shapes_temp{2} 'e' shapes_temp{3}]); % x-Koordinaten der Shapes
      shapes_sim{1,j}.r2(k) = str2double([shapes_temp{4} 'e' shapes_temp{5}]); % y-Koordinaten der Shapes
      shapes_sim{1,j}.r3(k) = str2double([shapes_temp{6} 'e' shapes_temp{7}]); % z-Koordinaten der Shapes
    end
  end

  %% Berechnen der MAC-Werte

  % Mode selection
  modes_meas = 1:1:5;
  modes_sim = 1:1:5;
  % Node selection
  nodes_meas = 1:48; % Node IDs in measurement
  nodes_sim = 1:48; % Node IDs in simulation

  % Berechnung der Gesamt-Eigenvektoren f¸r alle Moden
  for j=1:numel(modes_meas)
```

```
    freq_meas(j) = freq_meas_total(modes_meas(j)); % [Hz] Eigenfrequenzen der ausgew‰hlten Moden
    for k=1:numel(nodes_meas)
      IDs_meas(j,k) = find(shapes_meas{1,1}.nodeNum == nodes_meas(k));
      phi_meas(3*k-2:3*k,j) = [shapes_meas{1,modes_meas(j)}.r1(IDs_meas(j,k)) shapes_meas{1,modes_meas(j)}.r2(IDs_meas(j,k)) shapes_meas{1,modes_meas(j)}.r3(IDs_meas(j,k))]';
    end
  end
  for j=1:numel(modes_sim)
    freq_sim(j) = freq_sim_total(modes_sim(j)); % [Hz] Eigenfrequenzen der ausgew‰hlten Moden
    for k=1:numel(nodes_sim)
      IDs_sim(j,k) = find(shapes_sim{1,1}.nodeNum == nodes_sim(k));
      phi_sim(3*k-2:3*k,j) = [shapes_sim{1,modes_sim(j)}.r1(IDs_sim(j,k)) shapes_sim{1,modes_sim(j)}.r2(IDs_sim(j,k)) shapes_sim{1,modes_sim(j)}.r3(IDs_sim(j,k))]';
    end
  end

  % Berechnung der MAC-Matrix
  for j=1:numel(modes_meas)
    for k=1:numel(modes_sim)
      MAC(j,k) = Mac(phi_meas(:,j),phi_sim(:,k));
    end
  end

  %% Darstellung der MAC-Matrix

  treshold = 0;
  figure(1);
  h = imagesc(flipud(MAC'));
  colors = get(h,'CData');
  colors(colors < treshold) = treshold*63/64;
  set(h,'CData',colors)
```

```
set(gca, 'CLim', [0, 1]);
axis square;
%axis tight;
colormap([gray;jet]);
caxis([2*treshold-1 1])
cbar = colorbar;
set(cbar,'Limits',[treshold 1])
%title('MAC Matrix Pretest 15 MP', 'FontSize',12,'FontWeight','bold');
xlabel('Frequenzen Messung [Hz]');
ylabel('Frequenzen Simulation [Hz]');
set(gca,'XTick',1:numel(modes_meas),'XTickLabel',round(freq_meas,0),'Ticklength', [0 0]);
set(gca,'YTick',1:numel(modes_sim),'YTickLabel',round(fliplr(freq_sim),0),'Ticklength', [0 0]);
%xticklabel_rotate([],90,[],'Fontsize',11)
hold on
for i=1:numel(modes_meas)
   plot([i+0.5,i+0.5],[0.5,numel(modes_meas)+0.5],'k')
end
for i=1:numel(modes_sim)
   plot([0.5,numel(modes_sim)+0.5],[i+0.5,i+0.5],'k')
end

%% Funktion zur Berechnung der MAC-Matrix

function mAc=Mac(Phi1,Phi2)
% This function calculates mac between phi1 and phi2
mAc= (abs(Phi1'*Phi2))^2/((Phi1'*Phi1)*(Phi2'*Phi2));
end
```

Bibliography

[1] [ADH15] ADHIKARI, S. Free Vibration Analysis of Angle-ply composite plates with uncertain properties 17^{th} AIAA Non-Deterministic Approaches Conference Swansea University, United Kingdom, 2015

[2] [ALT18] ALTAIR, U. "Practical Aspects of Finite Element Simulation A Study Guide", 4^{th} Edition Released 07/2018

[3] [BIE12] BIERMANN, J. Vehicle Acoustics Reprint of lecture "Vehicle Acoustics"
Institut für Kraftfahrzeuge, RWTH Aachen University, Aachen, 2012

[4] [GUI06] GUILLAME,P. "Modal Analysis", Vrije Universiteit Brussel, Brussel, 2006

[5] [HAN51] HANSEN, C. "Fundamentals of acoustics", American Journal of Physics, 1951

[6] [HEI11] HEIßING, B., ERSOY, M. "Chassis Handbook Fundamentals, Driving Dynamics, Components, Mechatronics, Perspectives", Springer, Wiesbaden GmbH, 2011

[7] [HÜS18] HÜSKENS, P. LOHMANN, H. ECKSTEIN, L. VIEHÖFER, J., "EFEM in full-vehicle NVH-simulation considering lightweight components", Institut für Kraftfahrzeuge, RWTH Aachen University, Aachen, 2018

[8] [HÜS18] HÜSKENS, P., "Project report Modalanalyse Getriebebrücken – Ergänzende Untersuchungen", Institut für Kraftfahrzeuge, RWTH Aachen University, Aachen, 2018

[9] [MOE05] MOENS, D. VANDEPITTE, P., "Vibro-acoustic energy flow models implemented by finite elements", Department of Mechanical Engineering Leuven, Leuven, Belgium, 2005

[10] [RAI06] RAICHEL, D., "The Science and Applications of Acoustics", Second Edition, Springer, United States of America, 2006

[11] [SCH99] SCHWARZ, B., "Experimental Modal Analysis", CSI reliability week, Orlando, 1999

List of figures

List of equations